GOTOCORD

GOME Total Ozone Column Retrieval Development:

ESA ITT AO/1-4235/02/I-LG
ESRIN/Contract No. 16402/02/I-LG

WF-DOAS Algorithm Theoretical Basis Document

Issue 1.2

M. Coldewey-Egbers, M. Weber, L.N. Lamsal, R. de Beek,
M. Buchwitz, and J.P. Burrows

Institute of Environmental Physics, University of Bremen

Address:
Institute of Environmental Physics
Institute of Remote Sensing
University of Bremen FB1
P.O. Box 330 440
D-28334 Bremen
Germany

Contact:
Mark.Weber@uni-bremen.de

November 2003

Abstract

A novel total ozone retrieval algorithm that we call weighting function DOAS has been successfully implemented as an alternative approach to the standard DOAS (differential optical absorption spectroscopy) that is is currently operational in the GOME retrieval (Gome Data Processor Version 3.0). The weighting function DOAS method, abbreviated WF-DOAS, attempts to fit the vertical column density directly from the differential optical depth spectra and it can be applied to strong and weak absorption. This method has been demonstrated to be applicable to near-infrared trace gas column retrieval with SCIAMACHY and it has been adapted for total ozone retrieval in the near UV region. The processing of the GOME data is done in a non-linear least squares fitting using look-up-tables of reference intensities, weighting functions, and Ring spectra derived from the multiple scattering radiative transfer model SCIATRAN/CDI. Particular attention has been placed on proper modeling of the Ring effect that show significant dependence on the ozone profile shape due to molecular (ozone) filling-in. Other geophysical parameters such as effective albedo, cloud-top-height, cloud fraction, and effective height that are retrieved from GOME spectral information are used for the first time in combination to improve the ozone retrieval.

Contents

1 Introduction and Relevant Background

The GOME is the first European satellite experiment dedicated to global ozone measurements (Burrows *et al.*, 1999b). After eight years of operation (1995–2003) aboard the ERS-2 satellite it provides a unique long-term dataset. Combined with the TOMS dataset the satellite data record now extends to 25 years starting in 1978. GOME covers part of the data gap between 1994 and 1996, where no TOMS was available. Uncertainties in the continuation of the long-term downward trend in global ozone are partially related to this data gap and a possible bias between EP-TOMS (1996-present) and the earlier TOMS data record before 1994 (WMO Report, 1999). GOME and EP-TOMS have continued the ozone data record over the turn of the century. Both instruments show some sign of aging since early 2000 (Bramstedt *et al.*, 2003). Recently the tape recorder for intermediate data storage ceased functioning aboard ERS-2, limiting the coverage of GOME to parts of the northern hemisphere since June 2003.

In 2005 the first of a series of new GOME instruments (GOME2 generation) will be launched on the METOP series continuing long-term ozone monitoring in the next two decades. The current and future total ozone algorithms in use with GOME are also applicable to SCIAMACHY (launched 2002) and OMI (to be launched in 2004) (Bovensmann *et al.*, 1999; Stammes *et al.*, 1999). They may play an important role in continuing the data record into the METOP era.

From comparison with ground-based instruments (Lambert *et al.*, 1999; Lambert, 1995; Bramstedt *et al.*, 2003; GDP V3 VALREPORT, 2002), some shortcomings of the current GOME total ozone retrieval (GDP Version 3.0) remain. A seasonal cycle in the differences to ground-based data persists, but is reduced as compared to GDP V2.7 (Lambert *et al.*, 1999; GDP V3 VALREPORT, 2002). In addition, variation of this differences with solar zenith angle is still apparent in the GDP V3.0. Major changes from GDP V2.7 are the fitting of two ozone cross-sections at different temperatures and the introduction of an iterative airmass factor scheme based upon TOMS V7 profile shape climatology (Wellemeyer *et al.*, 1997).

In the standard DOAS approach, like the GDP V3.0, the slant column density is first derived from a spectral fit to the logarithm of the sun-normalized radiance and conversion into vertical column densities are done in a second step using airmass factors (AMF) calculated with radiative transfer models at a single wavelength. This approach assumes that the absorber is weak and the atmosphere optically thin. Ozone in the Huggins band shows significant absorption so that this basic assumption is violated.

In this study a new algorithm called WF-DOAS (weighting function DOAS), that has been first demonstrated to be applicable to trace-gas column retrieval in the near-infrared region of SCIAMACHY (Buchwitz *et al.*, 2000), was adapted to UV retrieval of total ozone and first results seem to indicate its promising potential (Coldewey-Egbers *et al.*, 2003). A prototype quasi-operational data processor using look–up tables for most RTM quantities such as reference intensities, weighting functions, and Ring spectra has been developed. In the WF-DOAS approach the vertical column is directly determined in the spectral fitting and it accounts for the variation of the air mass factor with wavelength.

Particular emphasis in the retrieval development was put on the use of the most appropriate Ring spectra by

including the effect of molecular filling-in, particularly, that from ozone itself using full radiative transfer modeling (Vountas *et al.*, 1998). Cloud information retrieved from the oxygen A-Band near 760 nm (Koelemeijer *et al.*, 2001) has been included in the retrieval. The ghost vertical column up to the cloud-top-pressure are estimated from the monthly zonal mean TOMS V8 climatology (G. Labow, private communication) to account for the missing ozone below the cloud.

For the first time several auxiliary quantities directly derived from the GOME spectral range such as cloud-top-height and cloud fraction (O2-A band) and effective albedo using the Lambertian equivalent reflectance (LER) near 377 nm (Herman and Celarier, 1997; Koelemeijer *et al.*, 2003) are used in combination as input to the ozone retrieval. The new algorithm has been validated by comparison with Dobson/Brewer data from the WOUDC database (Hare and Fioletov, 1998) in a similar fashion as described in Bramstedt *et al.* (2003) (see separate validation document). The goal of this study was to provide a novel algorithm which maintains a 1% relative consistency in the ozone record over the lifespan of GOME. Particularly comparison with selected ground based Brewer spectrometers show excellent agreement with differences to within $\pm 0.5\%$ in all seasons.

2 The GOME spectrometer

The GOME instrument is a double monochromator which combines a predisperser prism and a holographic grating in each of the four optical channels as dispersing elements The irradiance and radiance spectra are recorded with four linear Reticon Si-diode arrays with 1024 spectral elements each. Peltier elements attached to the diode arrays and connected to passive deep space radiators cool the detectors to about -40°C. Except for the scan mirror at the nadir view port, all spectrometer parts are fixed and the spectra are recorded simultaneously from 240 nm to 790 nm. The spectral resolution varies between 0.2nm (UV, Channel 1) and 0.4 nm (VIS, channel 4). In the releavnt spectral region for total ozone retrieval (Channel 2: 315nm–400 nm) the spectral resolution is about 0.17 nm but slightly varying across the channels. The oxygen A-band is measured in channel 4 near 760 nm and cloud information is derived from that band. Part of the light which reaches the predisperser prism is branched out and recorded with three broadband polarization measurement devices (PMD), which approximately cover the spectral range in channels 2 (300-400 nm), 3 (400-600 nm), and 4 (600-800 nm), respectively. The PMDs measure the amount of light at an instrument defined polarization angle.

The ERS-2 satellite moves in a retrograde, sun-synchronous, near polar orbit at a height of about 795km. The maximum scan width in the nadir viewing is 960km and global coverage is achieved within three days (after 43 Orbits). The local crossing time at the equator is 10:30am. An across track scan sequence consists of four ground pixel types called East, Nadir, West, and followed by a Backscan with 1.5 sec integration time each. In the majority of orbits the wide swath width is used meaning that each ground pixel type is 320 km across-track and 40 km along track (960 km across–track from East to West). On selected days smaller swath widths or static nadir positions are used (about 3 days per month).

A typical GOME orbit lasts about 100 min, half of which are spent in the night side of the earth. During this phase GOME carries out several sequences of dark current and LED measurements (pixel-to-pixel gain). Various temperature sensors spread over the entire focal plane assembly monitor the in-orbit temperature variations. Once a month, the internal calibration lamp, a Pt/Ne/Chr hollow cathode lamp, is switched on over an entire orbit. During this sequence a series of lamp measurements with and without the solar diffuser permits the investigation of long term degradation of the diffuser and to obtain an update of the wavelength calibration as a function of instrument temperature.

A typical GOME solar reference and earthshine spectrum covering Channel 1 and 2 are shown in Fig. 2.1. The bottom panels shows the corresponding backscattered reflectivity that is proportional to the sun-normalized radiance. The latter is inverted to retrieve ozone profiles and total ozone as well as other minor absorbers. In the current GOME Data Processor V3.0 (GDP V3.0) total ozone is retrieved from the spectral window 325–335 nm as indicated in Fig. 2.1.

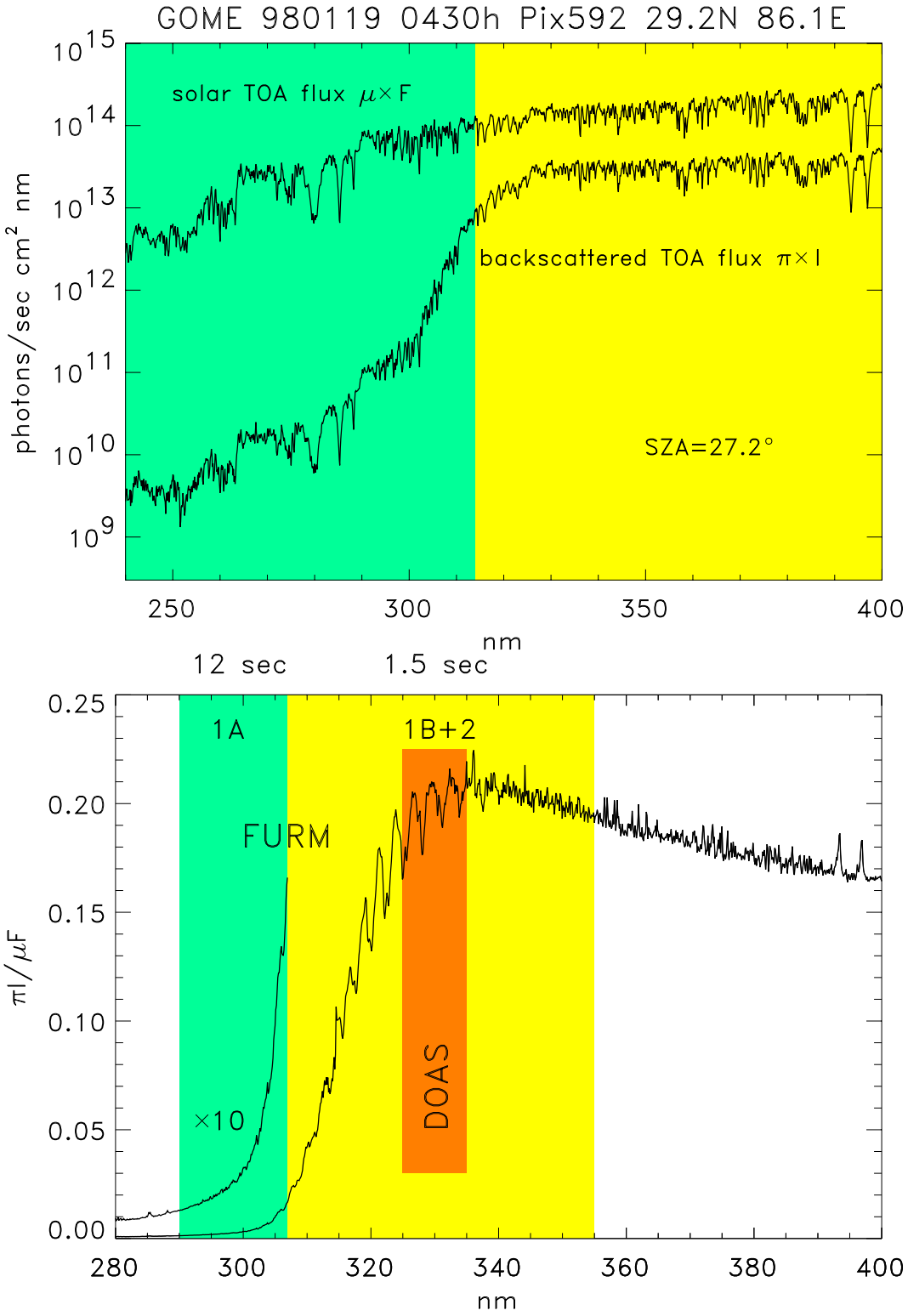

Figure 2.1: *Solar top–of–atmosphere (TOA) flux and backsacttered radiance spectra measured by GOME (top panel). Bottom panel shows the reflectiviy spectrum formed by ratioing backsattered radiance over solar reference. Green and yellow shadings in top panel show the different integration times used in different spectral regions: 12 sec in Channel 1a: 240-307 nm and after 1999 240-283 nm and 1.5 sec Channel 1a and channel 2 starting at 307nm/ 283 nm, respectively. Bottom panel shows the spectral DOAS window used for operational total ozone retrieval (325nm –335 nm, orange shading) and the range (290 nm –355 nm, green and yellow shading) used to derive ozone profiles as done, for instance, with the Full Retrieval Method FURM based upon an optimal estimation type algorithm (Hoogen* et al.*, 1999).*

3 WF-DOAS Total Ozone Algorithm

In this section we describe the new algorithm for retrieving total ozone from GOME. We start with a brief review of the standard DOAS approach and then give a description of our WF-DOAS algorithm.

3.1 Standard DOAS

Differential Optical Absorption Spectroscopy (DOAS) was developed for ground-based zenith-sky and long path measurements of atmospheric trace constituents (Platt and Perner, 1980). The GOME instrument launched in 1995 permits for the first time the DOAS method to be applied to space-borne observations (Burrows *et al.*, 1993, 1999b; GOME LVL2, 2000)

The space application of the DOAS algorithm to backscatter UV/visible measurements of up-welling radiances comprises of three steps. First the slant column density is obtained by fitting a superposition of molecular absorption cross-section spectrum and a polynomial to the measured intensity, i.e.

$$-\ln I^{mea}(\lambda) = \sum_{i}^{M} SCD_i \cdot \sigma_i(\lambda) + SCD_{Ring} \cdot \sigma_{Ring}(\lambda) + \sum_{k=0}^{n} a_k \, \lambda^k. \tag{3.1}$$

$I^{mea}(\lambda)$ is the measured sun-normalized radiance, M denotes the number of different molecules that have to be considered in the selected wavelength range, SCD_i are the molecular slant columns (fit parameters) and σ_i are the altitude independent absorption cross-sections. The polynomial function serves as a high pass filter and accounts for all broadband effects, e.g., scattering by molecules, aerosols and clouds. The Ring effect which arises from Raman scattering is treated as an effective absorber (see also Section 5 for a detailed discussion on the Ring effect).

In a second step the airmass factor (AMF) is used to convert the slant columns into vertical columns. The AMF has to be determined by radiative transfer calculations and it depends on several atmospheric parameters, such as sun-satellite geometry, surface albedo and ozone profile shape. As there is only one slant column per molecule for the entire fit window, there is only one AMF for this window. For optically thin atmospheres, the AMF is nearly wavelength independent. However, atmospheric ozone absorption between 325–335 nm is varying strongly and the AMF shows significant wavelength dependence, particularly, for large solar zenith angles. It should be noted here that a representative AMF wavelength can be found that minimizes this error for a specific fitting window (Burrows *et al.*, 1999b; GDP V3 VALREPORT, 2002).

The third step is a correction for cloud effects. Part of the ozone column below the cloud cannot be observed. In this case the obscured ghost vertical column is estimated using climatological values and has to be added to the retrieved column amount. In the current GDP (GOME Data Processor) Version 3.0, the oxygen-A-band transmittances are used to estimate the fractional cloud cover, but cloud-top-height is derived from a cloud climatology and/or empirical formula. (GOME LVL2, 2000).

The major improvement by going from V2.7 to GDP V3.0 is the use of two temperature cross-sections in the fitting to account for the ozone temperature and the introduction of the TOMS V7 total ozone dependent profile

climatology in an iterative air mass factor scheme (GDP V3 VALREPORT, 2002).

3.2 Weighting Function DOAS (WF-DOAS)

3.2.1 Theory

The weighting function DOAS algorithm (WF-DOAS) has been developed for trace gas retrieval in the near-infrared spectral range measured by SCIAMACHY (Buchwitz *et al.*, 2000) and it explicitly accounts for both weak and strong absorptions. Total column precisions have been estimated to be better than 1% for H_2O, CO_2, and CH_4, and better than 10% for N_2O and CO for SCIAMACHY. However, the algorithm is not limited to a particular wavelength range and molecular line absorbers. It is directly transferable to ozone retrieval in the ultraviolet spectral range requiring only fairly minor modifications.

The measured atmospheric optical depth is approximated by a Taylor expansion around the reference intensity plus a low-order polynomial. The total column information is obtained only from differential trace gas absorption structures as in case of standard DOAS. A polynomial P_i accounts for all broadband contributions. The WF-DOAS equation can be written as follows:

$$\begin{aligned}
\ln I_i^{mea}\left(V^t,\vec{b}^t\right) \approx\ & \ln I_i^{mod}\left(\bar{V},\bar{\vec{b}}\right) \\
& + \frac{\partial \ln I_i^{mod}}{\partial V}|_{\bar{V}} \times (\hat{V}-\bar{V}) \\
& + \sum_{j=1}^{F} \frac{\partial \ln I_i^{mod}}{\partial b_j}|_{\bar{b_j}} \times (\hat{b_j}-\bar{b_j}) \\
& + SCD_{Ring}\cdot\sigma_{i,Ring} \\
& + SCD_{usamp}\cdot\sigma_{i,usamp} \\
& + SCD_{I_0}\cdot\sigma_{i,I_0} \\
& + P_i
\end{aligned} \tag{3.2}$$

I^{mea} is the measured intensity and I^{mod} the reference intensity, as provided by the radiative transfer model. Index t denotes the true atmospheric state. The entire right-hand side of the equation (excluding the reference intensity) has to be adjusted to the measured intensity (left-hand side) for all spectral points (index i) simultaneously. $\bar{V}$ is the reference ozone column corresponding to the reference intensity, and$\hat{V}$ the retrieved vertical column. $\vec{b}$ contains all other atmospheric and surface parameters, such as interfering trace gases, temperature shift, and scalar albedo that can be simultaneously fitted.

All model parameters are denoted by over-bars ($\bar{}$), and all fit parameters are denoted by hats ($\hat{}$). The Ring effect, $\sigma_{i,Ring}$, the I_*o* effect, σ_{i,I_0} (Aliwell *et al.*, 2002), and the under-sampling correction, $\sigma_{i,usamp}$ (Slijkhuis *et al.*, 1999), are treated as effective slant absorbers similar to the approach used in standard DOAS[1]. Slant

[1]The I_o effect describes the effect of measuring cross-sections with the sun as a source that is highly structured as opposed to a continous light source like in a laboratory set-up. The undersampling correction models the low sampling rate that is inherent to GOME which has a full-width-of-half–maximum intrument function that is 1.5 detetor pixels wide. The correction is determined by simulating the undersampling using high resolution solar reference data and convolving it with the appropriate instrument function

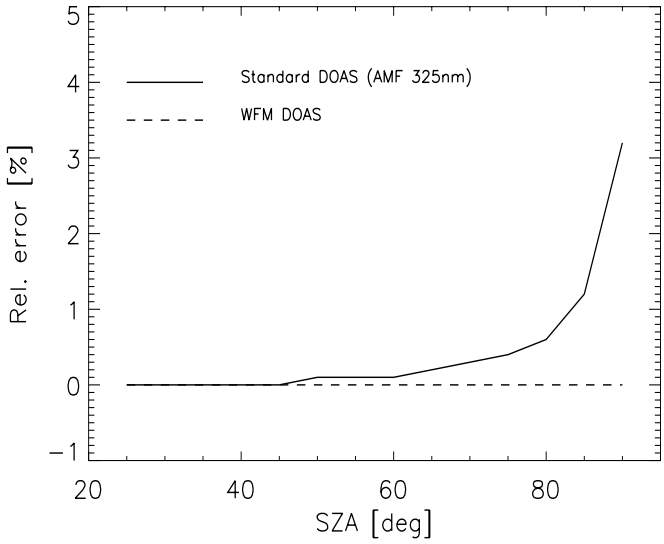

Figure 3.1: *Comparison between standard DOAS using one single AMF (325 nm) and WF-DOAS using wavelength dependent weighting functions. Synthetic spectra were computed for one atmospheric scenario (total ozone* $= 275$ *DU, mid-latitude profile shape from TOMS V7, altitude* $= 0$ *km, albedo* $= 0.05$*, and LOS* $= 0°$*) and varying solar zenith angles from 25° to 90° in 5° steps. We used the correct reference scenarios for WF DOAS retrieval to avoid errors due to a-priori assumptions on atmospheric parameters.*

column fitting can be also applied to minor absorbers such as NO_2 and BrO, thereby, avoiding look-up-tables for these gases.

The main difference between the WF-DOAS algorithm and the standard DOAS algorithm is the use of wavelength dependent trace gas weighting functions instead of absorption cross-sections and air mass factors. Weighting functions (WF) describe the relative radiance change due to a vertical profile change assuming an altitude independent scaling factor ($WF = \frac{\partial I}{I} / \frac{\partial V}{V}$). Figure 3.1 shows a comparison between standard DOAS and WF-DOAS using synthetic spectra to demonstrate the influence of the wavelength dependent WFs compared to one single AMF, here 325 nm like in GDP V3.0. Errors may reach a few percent for large solar zenith angles.

The need for an airmass factor conversion is eliminated in the new algorithm as the fit parameters are the vertical columns. By introducing additional terms in vector $\vec{b}$, for instance the temperature shift weighting function, the algorithm accounts for temperature dependence of the ozone absorption.

The unknown fit parameters are derived using a linear least-squares minimization:

$$\|\vec{y} - \tilde{A}\,\vec{x}\|^2 \rightarrow \min \qquad \Longrightarrow \qquad \hat{\vec{x}} = \tilde{C}_x\,\tilde{A}^T\,\vec{y}.$$

Vector $\vec{x}$ contains the fit parameters $\bar{V}$, $\bar{b_j}$ and the polynomial coefficients. The weighting functions and the polynomial basis functions are contained in matrix $\tilde{A}$. $\vec{y}$ contains the difference between the logarithm of measured intensity and the reference intensity.

Table 3.1: *Parameter space of the look-up-tables. (*) min/max of relative azimuth angle depend on SZA and LOS (see Figure 3.3).*

Atmospheric Parameter	Min	Max	Δ	N
Total Ozone (high latitudes)	125 DU	575 DU	50 DU	10
Total Ozone (mid latitudes)	125 DU	575 DU	50 DU	10
Total Ozone (low latitudes)	225 DU	475 DU	50 DU	6
Solar Zenith Angle	15°	92°	5° if SZA $\leq$ 70° 1° if SZA $>$ 70°	34
Line-Of-Sight	-34.5°	34.5°	11.5°	7
Relative Azimuth Angle	(*)	(*)		3
Surface Albedo	0.02	0.98	$\sim$ 0.2	6
Altitude	0 km	12 km	2 km	7

3.2.2 Reference spectra

Online radiative transfer model calculations as part of the data processing are quite computational expensive. All RTM quantities have, therefore, been collected into a look-up-table. A large set of reference spectra has been constructed, which includes nearly all possible atmospheric conditions. The radiance spectra and weighting functions are computed as a function of total ozone including profile shape from TOMS V7 (Wellemeyer *et al.*, 1997), solar zenith angle (SZA), line-of-sight (LOS), relative azimuth angle (RAZ), surface albedo a_o, and altitude h. The SCIATRAN/CDI code, an extension of the GOMETRAN++ radiative transfer model (Rozanov *et al.*, 1997, 1998), was used which enables altitude-resolved weighting functions to be determined quasi-analytically with only a negligible amount of additional computer effort (Rozanov *et al.*, 1998). SCIATRAN/CDI was specifically developed for simulation of back-scattered intensities and is based on the finite difference approach.

Table 3.1 gives an overview of the parameter space. Ozone and temperature profiles are taken from TOMS Version 7 climatology which contains different profile shapes for three latitude belts (low, middle and high) as a function of the total ozone column (Wellemeyer *et al.*, 1997) (see also Appendix A).

Minimum and maximum values of the relative azimuth angle depend on solar zenith angle and line-of-sight. Figure 3.3 shows its dependence on both parameters. It has been obtained using all GOME orbits from 1998. The minimum, maximum, and mean angles are taken for reference spectra calculation for a given combination of solar zenith angle and line-of-sight.

Altitude of the boundary in the lower atmosphere varies between 0 km and 12 km. In the actual retrieval this altitude is identified with the effective height derived from the GOME scene. The effective height is a weighted sum of surface altitude h_o and cloud top height h_{cld}, with cloud fraction f as a weighting factor (see Section 4.2 for more details). Particularly in the tropics values above 10 km can be reached in the inner tropical convergence zone (ITC, see Fig. 3.2). Therefore, our reference altitude grid contains an upper limit of 12 km.

Each GOME ground pixel extends 320 km across scan and the line-of-sight varies from $\pm$34.5° to $\pm$11.5° for east and west pixels and from -11.5° to 11.5° for nadir pixels. The use of only one reference spectrum for the entire pixel (e.g. at 23.0°) leads to spectral structures compared to a high resolved scan which result

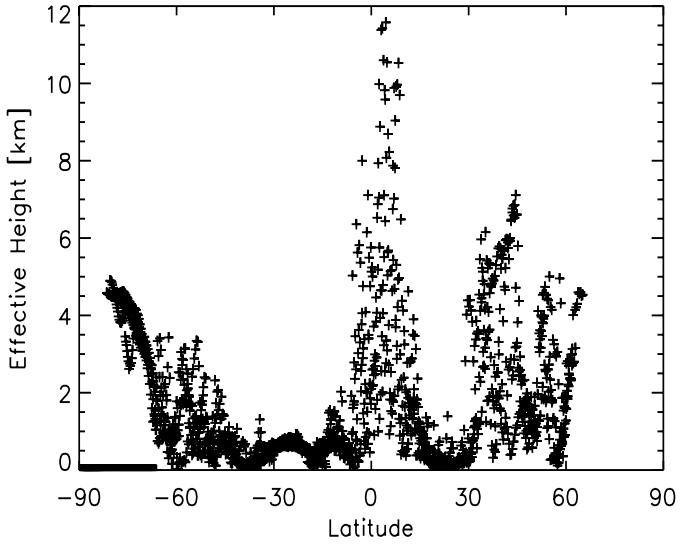

Figure 3.2: *Effective height as a function of latitude for GOME orbit 60108013 (8th January 1996). The innertropical convergence zone (ITCZ) is identified by effective heights close to 12 km.*

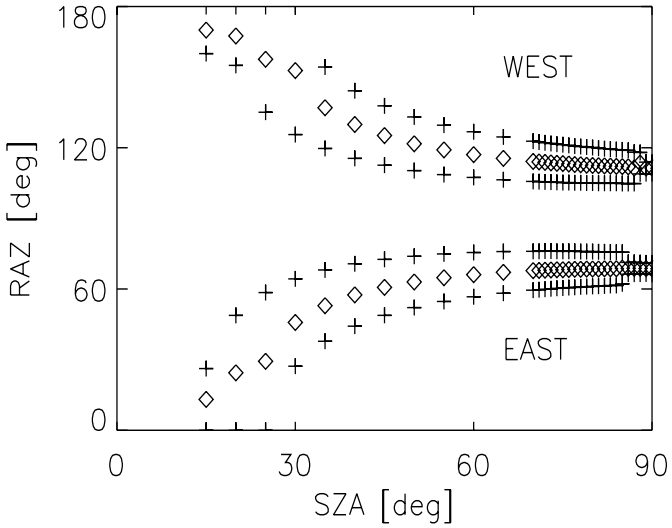

Figure 3.3: *Dependence of relative azimuth angle on solar zenith angle and line-of-sight. Crosses denote the minimum and maximum angles and diamonds the mean angles. All GOME data from 1998 were taken into account.*

in non-negligible vertical column errors. We decided to calculate three reference spectra (R_1, R_2, R_3) for three different angles (at begin, middle, and the end of integration) for each pixel. Those three intensities and weighting functions are then averaged as follows to obtain a good estimate of the mean across the ground pixel.

$$\bar{R} = \frac{1}{6} R_1 + \frac{4}{6} R_2 + \frac{1}{6} R_3. \tag{3.3}$$

Studies using synthetic data have shown, that three reference points for each pixel are sufficient. Using more than three spectra per pixel only slightly reduces the vertical column error.

The reference spectra are computed for discrete solar zenith angles (see Table 3.1). The intensity and weighting functions vary nonlinearly between two angles, particularly beyond 70°. Studies with synthetic spectra indicated that vertical column errors reach 1.2% at 89° when linear interpolated in a 1° step table. Therefore, the solar zenith angle dependence of the reference intensities has been fitted to Chebyshev polynomials and the polynomial coefficients are stored in the look-up-table. The interpolation error can be reduced to $< 0.1\%$ for SZA up to 90° using 22 terms in the expansion.

Each reference spectrum contains sun-normalized radiances and weighting functions for O_3 and temperature shift in the spectral region 323 nm-337 nm. The temperature weighting function expresses the radiance change for a given shift ΔT of the temperature profile. The WF-DOAS algorithm interpolates in the multi-dimensional look-up-table (LUT) to find the appropriate reference and weighting function spectra in the non-linear least–squares fitting.

3.2.3 Pseudo-spherical approximation

All reference spectra have been computed with SCIATRAN/CDI in the pseudo-spherical approximation. Compared to the full spherical mode, errors in radiances may arise, particularly towards the swath edges. Those radiance errors translate in vertical column errors. It can be, however, shown that by using viewing angles (line-of-sight and solar zenith angle) at the ground level rather than top-of-atmosphere as done in GDP V3.0 retrieval, the pseudo-spherical (PS) approximation leads to negligible slant column errors even up to 46° line-of-sight, which is the maximum line-of-sight planned for GOME-2 aboard METOP (Kerridge *et al.*, 2002). In Figure 3.4 the difference of the various pseudo-spheric approximations relative to a spherical RTM at 46° (West pixel) is shown. The ground level viewing geometry used in the PS approximation leads to virtually no differential structures in the differences.

3.2.4 Nonlinear fit

A *shift-and-squeeze* of individual spectra can be carried out to improve wavelength misregistration between weighting functions (or cross-sections), radiances, and solar reference spectrum. The earthshine spectrum as well as the reference intensity and weighting functions can be translated in wavelength by a single value (*shift*), and stretched or compressed by a single value (*squeeze*) about some reference wavelength λ_{ref}. The *shift-and-squeeze* can be written as follows:

$$\lambda' = \lambda + shift + (squeeze - 1) \cdot (\lambda - \lambda_{ref}). \tag{3.4}$$

The entire right hand side of Eq. 3.2 depends non-linearly on the *shift-and-squeeze* parameter pairs, which must be determined iteratively using a non-linear least squares method. The linear regression is now embedded in the non-linear fitting, and must be performed at each iteration. Once the non-linear fit has converged, another linear regression is performed to establish the final values of the fitting parameters.

Following the recommendation of M. van Roozendael (Roozendael *et al.*, 2003), a constant shift of +0.017 nm has been applied to GOME FM cross sections for ozone and nitrogen dioxide (Burrows *et al.*, 1998, 1999a) before the calculation of reference spectra and weighting functions. This permits the limitation of the shift and squeeze operation to the earthshine spectrum.

In order to correct for the observed Doppler shift (+0.008nm) in the solar reference and for wavelength calibration errors using the onboard Pt/Ne/Cr hallow cathode lamp, the GOME solar spectrum is nonlinearly fitted to a high- resolution solar atlas derived from Fourier transform spectrometer measurements carried out with the McMath Solar Telescope, Kitt Peak Observatory, Arizona (Kurucz *et al.*, 1984). This is done before the DOAS fit is performed. This wavelength re-calibration is termed the Fraunhofer fit and its implementation reduces the residual RMS by about 10%. Figure 3.5 (left panel) shows the ratio of the fit RMS with and without Fraunhofer shift versus total ozone column. The right panel shows the retrieved ozone with and without Fraunhofer shift. The Fraunhofer fit results in a nearly constant increase of about 2%. We used all GOME over-passes at BelgranoII Station (Antarctica, 77.87°S, 34.63°W) from September to December 1997 in these figures.

3.2.5 Spectral fit window

We selected the 8.2 nm wide fit window from 326.6–335.0 nm for ozone retrieval. There is a non-negligible correlation between ozone and temperature shift weighting function and it should be minimized when retrieving both parameters simultaneously. Figure 3.6 shows the correlation coefficient as function of window width for a start wavelength of 326.6 nm. It decreases with increasing window width. In Section 8.4 we investigate the influence of other combinations of fitting window sizes and start wavelengths.

3.2.6 Albedo weighting function

Similar to the scalar temperature shift weighting function, it might be possible to retrieve an effective albedo by including the albedo weighting function in the fit. This has been tested with synthetic spectra that have been modeled for different solar zenith angles (45°and 75°), two albedos (0.08 and 0.75) and two ozone amounts (300 DU and 355 DU). These spectra were simulating the measurements. Reference radiances were simulated for albedo values of 0.05, 0.1, 0.7 and 0.8, and ozone amounts of 275 DU, 325 DU and 375 DU.

Fit results with and without albedo weighting function are presented in Figure 3.7. If albedo weighting function is included in the fit, errors reach $\pm 2\%$. The retrieved values for albedo are mostly unphysical, i.e. negative or greater than one. If albedo weighting function is not included in the fit and linear interpolation between reference spectra is performed, errors are small ($\pm$ 0.2 %).

The rather poor results can be explained by the strong correlation between ozone and albedo weighting functions, as depicted in Fig. 3.8. The correlation coefficient is 0.98. It is not recommended to retrieve both

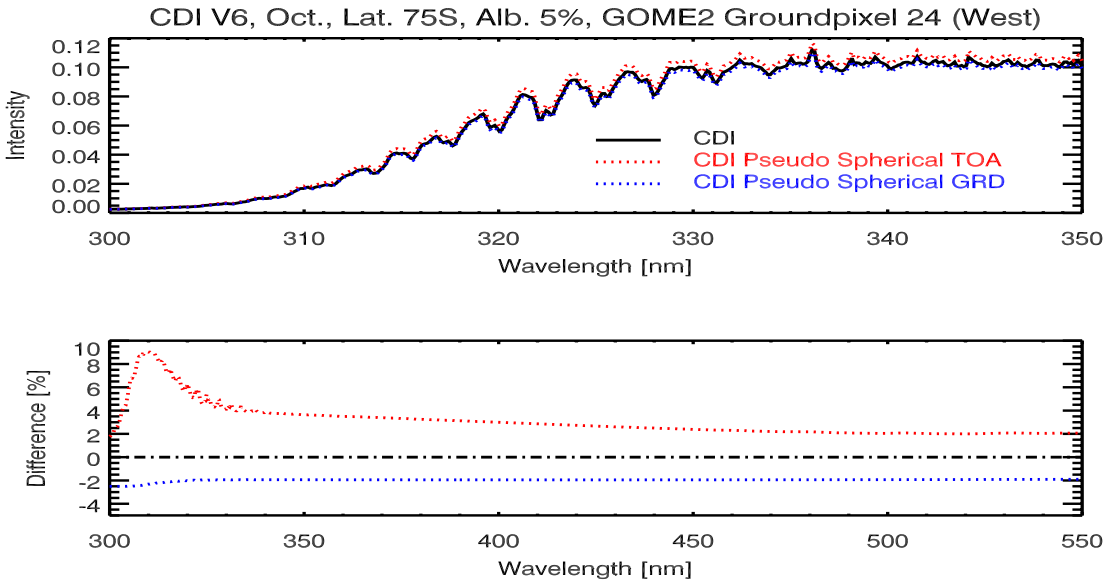

Figure 3.4: *Differences in top-of-atmosphere radiances using different viewing geometries in the pseudo-spherical multiple scattering RTM. Results are shown for maximum line-of–sight planned for GOME-2 aboard METOP (46°). Black: Full spherical calculation with SCIATRAN/CDI, Blue: pseudo-spherical approximation using line-of-sight and solar zenith angle at the ground, Red: pseudo-spherical approximation using line-of-sight and solar zenith angle at top-of-atmosphere. Top panel: radiance spectrum, bottom panel: differences to spherical model. Taken from Kerridge* et al. *(2002).*

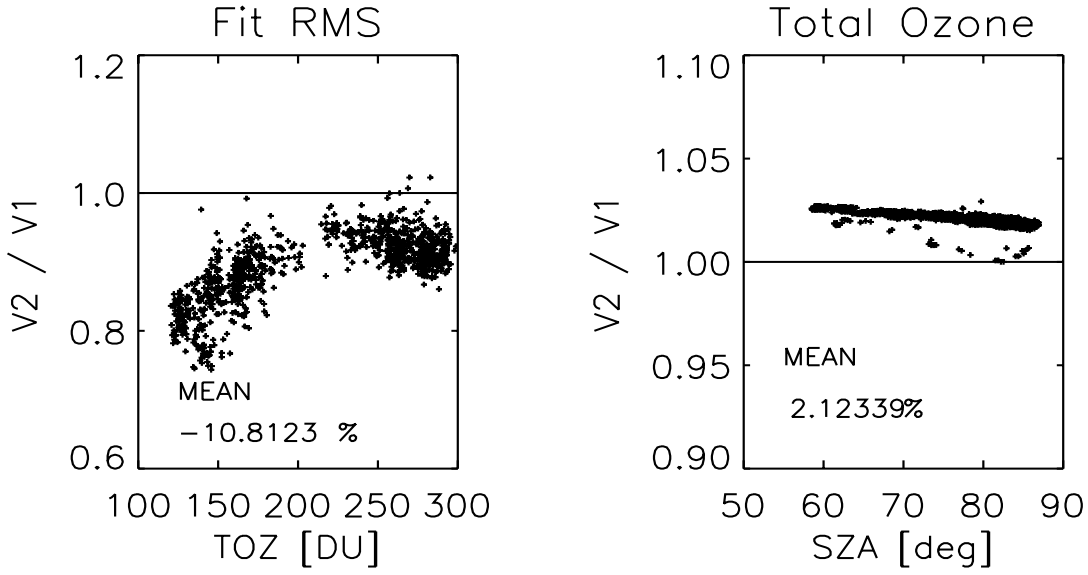

Figure 3.5: *Retrieval results with and without shift and squeeze of the GOME solar spectrum to Kurucz spectrum. Left: Ratio of fit RMS with and without shift versus total ozone, and right : ratio of total ozone columns with and without shift versus solar zenith angle. All GOME over-passes at BelgranoII Station (Antarctica, 77.87° S, 34.63° W) were taken into account.*

parameters simultaneously. Nevertheless accurate albedo values are needed for selecting the proper reference scenario from the look-up-tables. The albedo values are not retrieved in the ozone fitting window, but instead derived from an absorption free region near 377 nm (see Section 4.3).

3.3 Cloud correction

In case of cloud contaminated ground pixels, the part of the ozone column, which is below the top of the clouds, cannot be detected by the satellite. This ghost vertical column (GVC) has to be estimated from climatological vertical ozone profiles and is then added to the vertical column retrieved from the spectral fit.

The GVC is computed by integrating the profile $O_3(p)$ from pressure $p(h_o)$ at the surface altitude h_o up to the cloud top pressure $p(h_{\mathsf{cld}})$. Partial cloudiness can be taken into account by multiplying the integrated partial column with fractional cloud cover f as follows:

$$\mathrm{GVC} = f \cdot \int_{p(h_o)}^{p(h_{\mathsf{cld}})} O_3(p)\, dp. \tag{3.5}$$

Cloud fraction and cloud top pressure are derived using the FRESCO algorithm from Koelemeijer *et al.* (2001), which uses the oxygen A-band transmittances from GOME.

Ozone profiles used in the GVC calculation come from TOMS V8 monthly zonal mean climatology (G. Labow, NASA–GSFC, private communication). The data base contains profiles for 18 latitude bands (10°). Since tropospheric ozone has a seasonal cycle due to biomass burning and other seasonal pollution events it is believed that a monthly zonal mean climatology provides a slightly better estimate for tropospheric ozone although tropospheric plumes will be averaged while taking zonal means. Nevertheless, compared to TOMS V7 climatology which we use for our reference data base, V8 takes hemispherical and seasonal differences into account. Figure 3.9 shows for two GOME orbits from January and April 1996 the differences between both climatologies in determing the GVC as a function of latitude. In northern hemisphere the GSFC climatology for GVC estimation leads to higher values and in southern hemisphere, GVC is smaller using TOMS V8 zonal monthly means instead of TOMS V7 profiles.

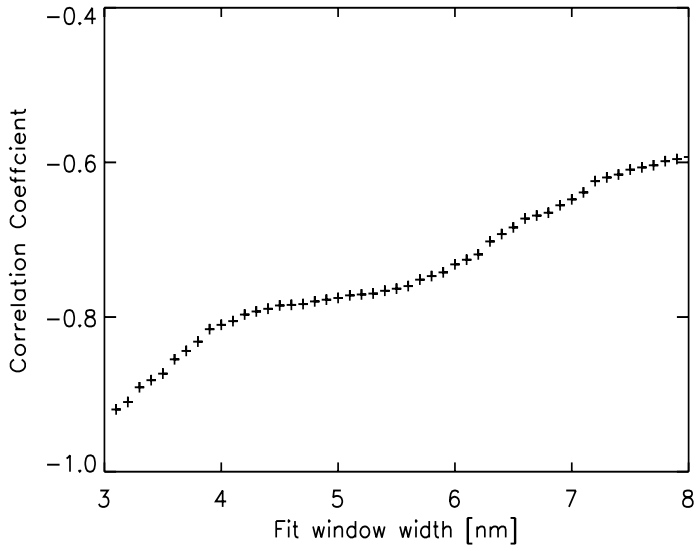

Figure 3.6: *Correlation coefficient as a function of window width and a start wavelength of 326.6 nm.*

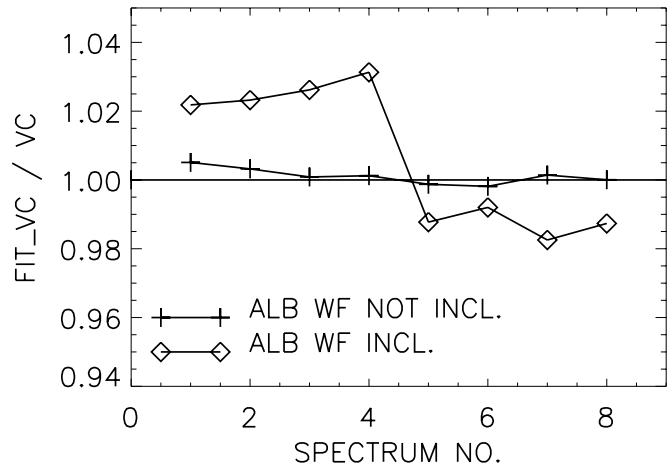

Figure 3.7: *Ratio of fitted vertical column for different albedo scenarios. Crosses denote fits without albedo weighting function and diamonds fits which included the albedo weighting function.*

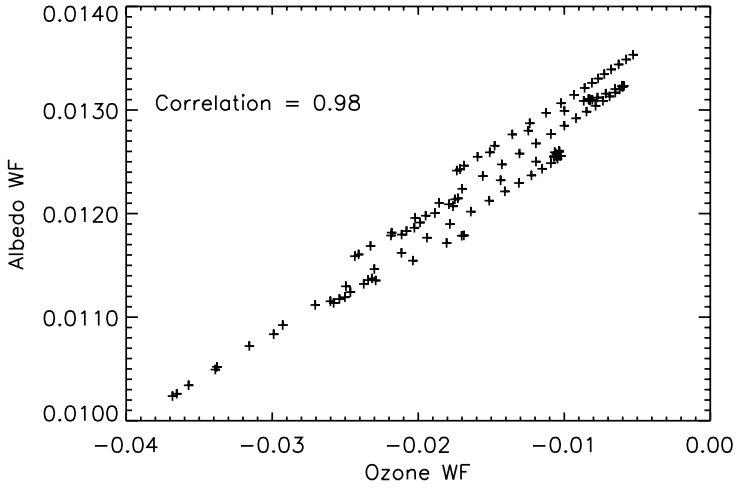

Figure 3.8: *Correlation between albedo and ozone weighting functions. Correlation coefficient is 0.98 in the fit window 326.6 - 335.0 nm.*

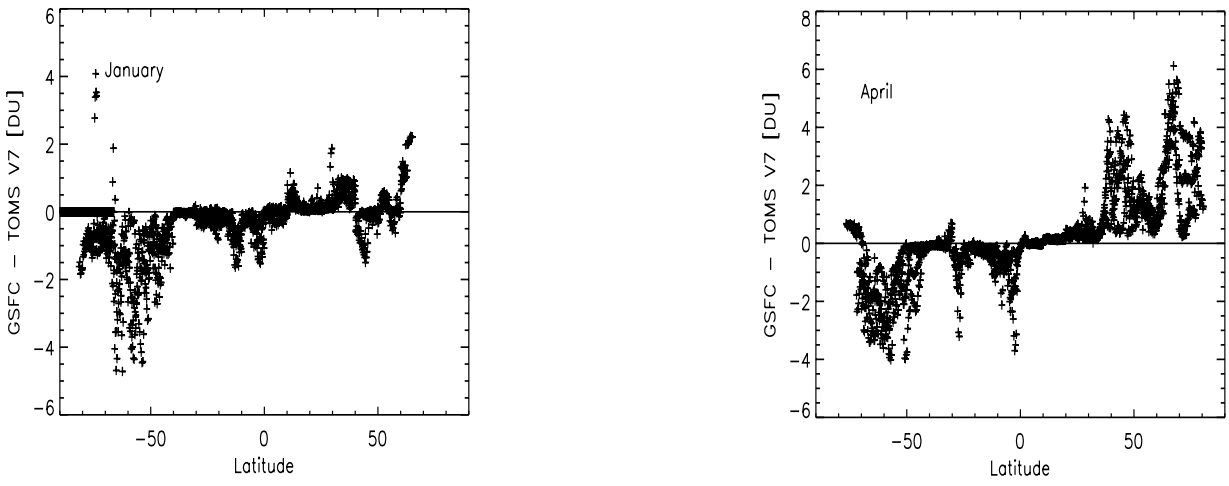

Figure 3.9: *Differences in GVC calculated with TOMS V7 and TOMS V8 zonal and monthly mean climatology for the GOME orbits 60108013 (left) and 60401123 (right) observed in January and April 1996.*

4 Retrieval Schemes

This section describes the various retrievals (cloud parameters and effective albedo) that are needed to prepare WF-DOAS. The iterative WF-DOAS scheme is described at the end of this Section.

4.1 Summary of WF-DOAS Retrieval Input

For WF-DOAS the following data and information are required:

- Calibrated GOME level 1 radiance spectrum (earthshine spectrum) and GOME solar data from the same day
- GOME ground pixel geolocation information (latitude and longitudes of pixel center and corners of footprint)
- GOME top-of-atmosphere viewing geometry (solar zenith angle, line-of-sight and relative azimuth angles) that is converted into ground level angles.
- *A priori* value for total ozone from GOME level 2 data (GDP V3.0)
- Effective altitude, which is obtained from FRESCO output (see section 4.2)
- Effective albedo, which is obtained from GOME level 1 radiance and irradiance data at 377 nm (see section 4.3)

4.2 Effective altitude from FRESCO

Effective altitude is obtained from FRESCO (Fast Retrieval Scheme for Clouds from the Oxygen A-Band) Koelemeijer *et al.* (2001). This algorithm derives the cloud-top height and the cloud fraction from the oxygen transmittance, assuming a high reflecting boundary representing the cloud top. The surface albedo a_b is taken from minimum spectral reflectances derived from a five year GOME data record (Koelemeijer *et al.*, 2003). For the cloud-top albedo a value of 0.8 is assumed. FRESCO differs from the ICFA (Initial Cloud Fitting Algorithm) (GOME LVL2, 2000) used in GDP V3.0 in the way that the latter retrieves the surface albedo as a second parameter after the cloud fraction while the the cloud-top-height as a function of latitude remains fixed. In contrast, FRESCO keeps the albedo values for both surface and cloud fixed during the fit. It should be noted here that the retrieved cloud-top-height and cloud fraction from FRESCO represents effective parameters for the spatial resolution of the GOME observations that offer the best TOA radiance estimate (indepenedent pixel approximation).

The effective height for the GOME ground pixel is a weighted sum of the ground altitude and the retrieved cloud top height weighted by the fractional cloud cover. Surface pressure and cloud top pressure from FRESCO output are converted into altitudes (surface height h_o and cloud top height h_{cld}) using US standard atmosphere.

Table 4.1: *LUT parameter space for LER retrieval*

Parameter		Grid Points
Altitude	[km]	0.0, 0.5, 1.1, 2.1, 3.3, 4.7, 6.0
LOS	[°]	0.0, ±6.0, ±7.0, ±15.0, ±22.5, ±23.5, ±30.0, ±35.0, ±40.0
RAZ	[°]	0.0°- 180.0°in steps of 10.0°
SZA	[°]	0.0, 10.0, 20.0, 30.0, 35.0, 40.0, 45.0, 50.0, 55.0, 60.0, 65.0, 70.0, 73.0, 76.0, 78.0, 80.0, 81.0, 82.0, 83.0, 84.0, 85.0, 86.0, 87.0, 88.0, 89.0, 90.0
Albedo	[-]	0.00, 0.02, 0.04, 0.06, 0.10, 0.15, 0.20, 0.30, 0.45, 0.60, 0.80, 1.0

The effective altitude is then defined as:

$$h_{\mathsf{eff}} = f \cdot h_{\mathsf{cld}} + (1 - f) \cdot h_o. \tag{4.1}$$

In the snow and ice mode, the effective altitude is the value which comes out as the effective altitude for the reflecting layer assuming $f = 1$. The cloud discrimination only works if an albedo contrast exists between surface and cloud ($a_o \neq a_{\mathsf{cld}}$).

Fig. 4.1 shows the total ozone ratio from retrieval including effective altitude and without effective altitude (ground altitude was assumed instead). The use of the effective height tends to decrease the retrieved ozone by up to 5%.

4.3 Effective albedo algorithm

The Lambertian Equivalent Reflectivity (LER) (Herman and Celarier, 1997) defines the effective albedo and is obtained from GOME sun-normalized radiance at 377.6 nm. This wavelength was selected since it shows very small variation with respect to the Ring effect that can be easily corrected for. A look-up-table of pre-calculated sun-normalized radiances as a function on solar zenith angle, line-of-sight, relative azimuth angle, ground altitude, and surface albedo (see Table 4.1 for parameter space) at this wavelength has been generated using SCIATRAN/CDI (Menkhaus *et al.*, 1999).

The viewing geometries (SZA, LOS and RAZ) are taken from GOME observations. Altitude input is the effective altitude from FRESCO (see section 4.2). For this set of parameters, radiances as a function of albedo are extracted from the table. The effective albedo is obtained by bi-sectional search along this curve as schematically shown in Fig. 4.2. Figure 4.3 shows all GOME measured TOA reflectivities from July 1998 as a function of the retrieved LER. For high values in case of cloud contaminated pixels or snow and ice coverage both are nearly identical. The TOA reflectivity does not go to zero near zero effective albedo (LER) due to Rayleigh scattering. Mie scattering due to aerosols also modifies the TOA reflectivity. The use of the LER in the retrieval does to a certain extent represents a first order aerosol correction, except for absorbing aerosols that may prevent ozone below the aerosol layer from being detected (Hsu *et al.*, 1999) (see also Section 7.1).

In Figure 4.4 the concept of effective height and partial ozone column below the cloud is schematically shown.

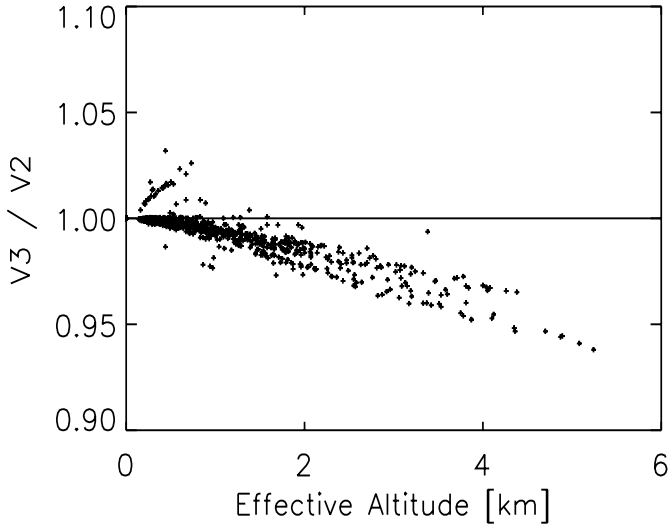

Figure 4.1: *Ratio of total ozone retrieval with and without effective altitude for all GOME overpasses at BelgranoII Station (Antarctica) from September to December 1997.*

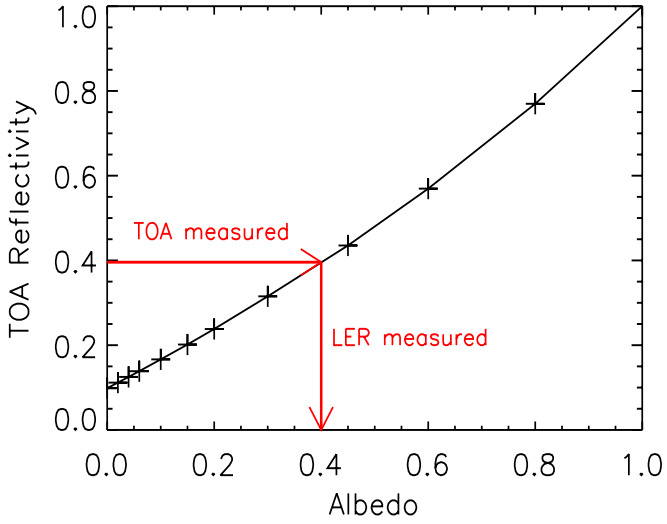

Figure 4.2: *Schematics of LER estimation. TOA reflectivity is plotted as a function of albedo for a fixed scenario (SZA, LOS, RAZ and altitude) and the effective albedo is derived from bi-sectional search along this curve*

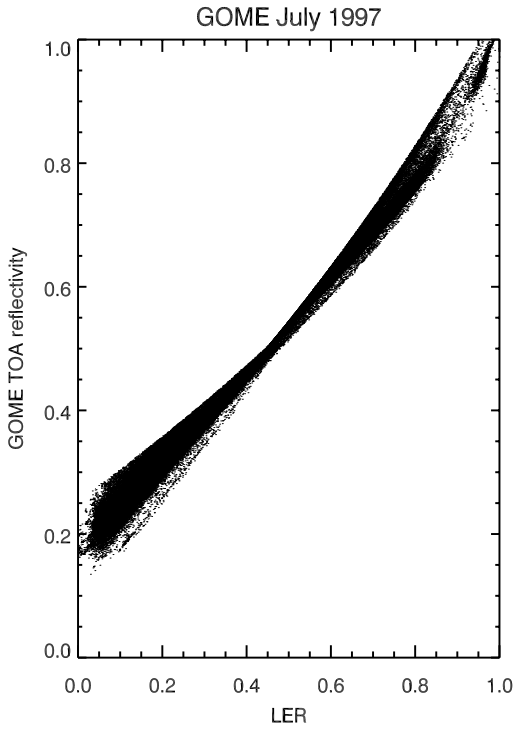

Figure 4.3: *GOME measured TOA reflectivity versus retrieved LER for all data from July 1998.*

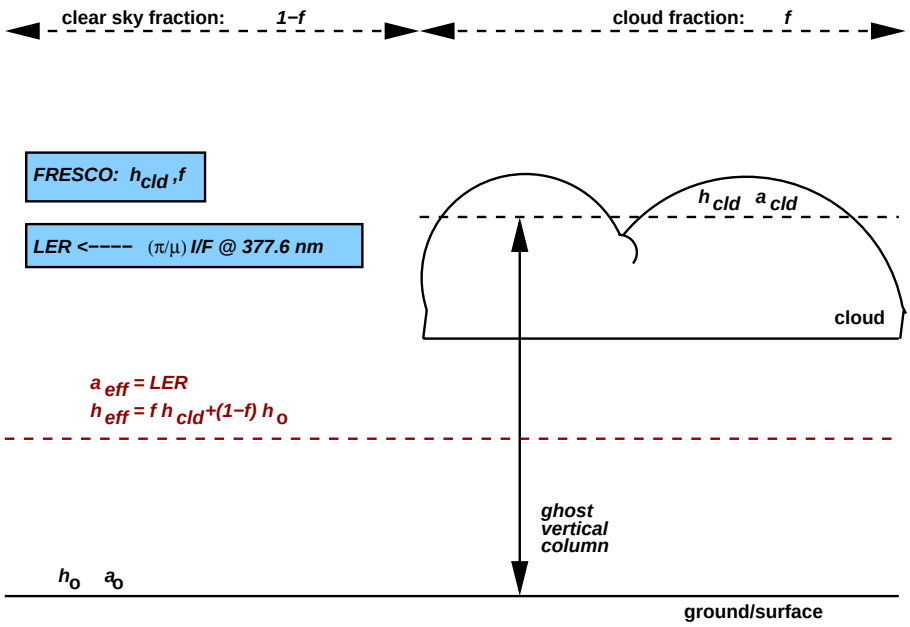

Figure 4.4: *Schematics of concept of effective height and ghost vertical column (see explanation in text).*

4.4 Iterative WF-DOAS scheme

The algorithm contains an iterative scheme to retrieve total ozone. The first step is to find the nearest neighbor reference scenario. As a first guess the scenario which most closely matches the vertical column derived from operational algorithm GDP V3.0 is selected. Alternatively, one could start with a climatological value. Linear interpolation between effective albedo, effective altitude and relative azimuth angle is performed to obtain the closest reference.

The next step is to find the nearest Ring spectrum in the same manner. They have been calculated only for nadir geometry and no interpolation will be performed for albedo and altitude.

After the spectral fitting the retrieved ozone column is compared with that of the reference scenario and the fit is repeated if a reference scenario can be found which is closer to the retrieved value. A schematics of the algorithm is shown in Figure 4.5. After the iterations stops the ghost vertical column is added to the retrieved column to obtain the final total ozone column amount.

4.5 WF-DOAS Version 1.0

In WF-DOAS Version 1.0 the spectral window 326.6 nm - 335 nm is used in the fitting procedure. In addition to ozone vertical column, the temperature shift is retrieved. NO_2 , BrO, Ring, and undersampling corrections are treated as effective SCD. It should be noted here that the reference database for radiances and weighting function has not been derived using the I_o corrected ozone cross-sections. In order to include this effect a difference spectrum of the GOME FM 98 cross-sections with and without the I_o correction (courtesy of M. van Roozendael) has been used as an effective absorber. Some preliminary analysis confirmed the -0.2% decrease in total column as observed in GDP V3 VALREPORT (2002). The I_o correction leads to a very small corrections of the ozone columns (below 0.2%) and is not included in this version (optional). A cubic polynomial is fitted to obtain differential optical depths.

In the following sections this basic setting has been applied in the GOME retrieval. Typical fitting residuals are shown in Fig. 4.6, where the differential optical depth measured and modeled as well as the contribution of the individual terms in the DOAS equation are shown. BrO has in most cases negligible contributions except for those region with enhanced tropospheric BrO (Richter *et al.*, 1998, see for instance). The RMS of the fit residuals is usually on the order of 0.001 which is about half the typical values achieved in GDP V3.0.

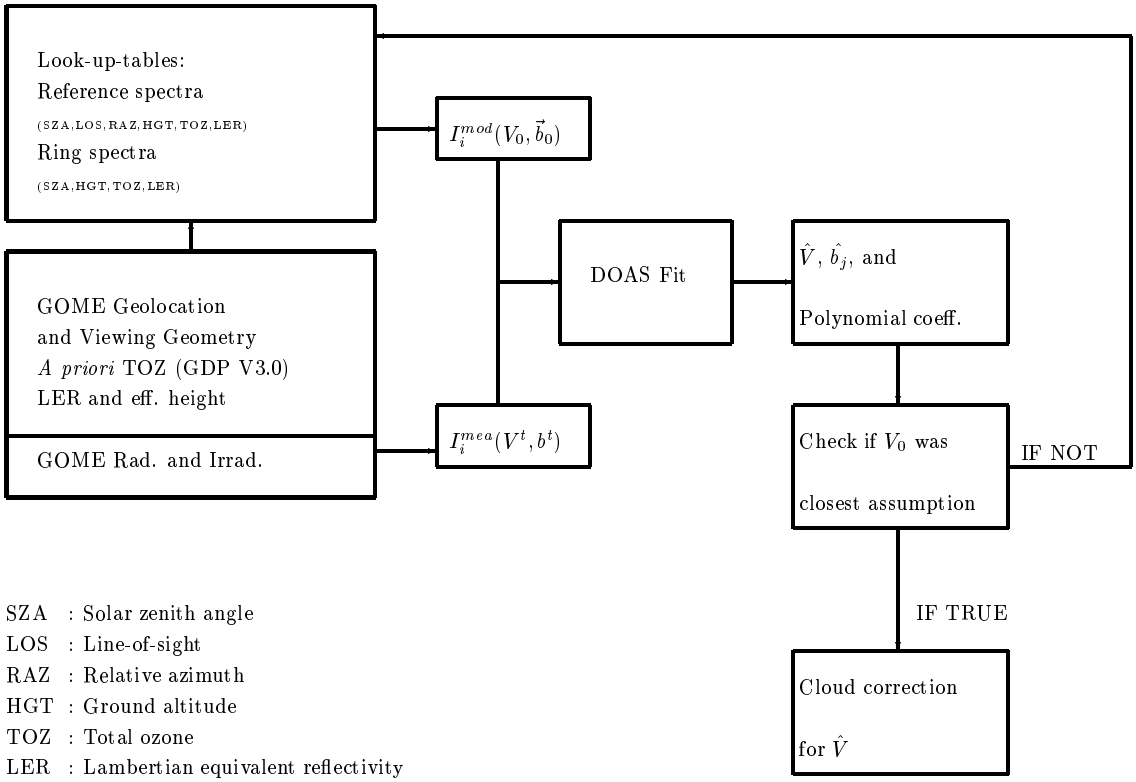

Figure 4.5: *Scheme of iterative WF-DOAS scheme. V_0 is the total column amount from the reference scenario. If this value is not the closest grid-point to the retrieved column $\hat{V}$, the fit is repeated by selecting a new reference scenario.*

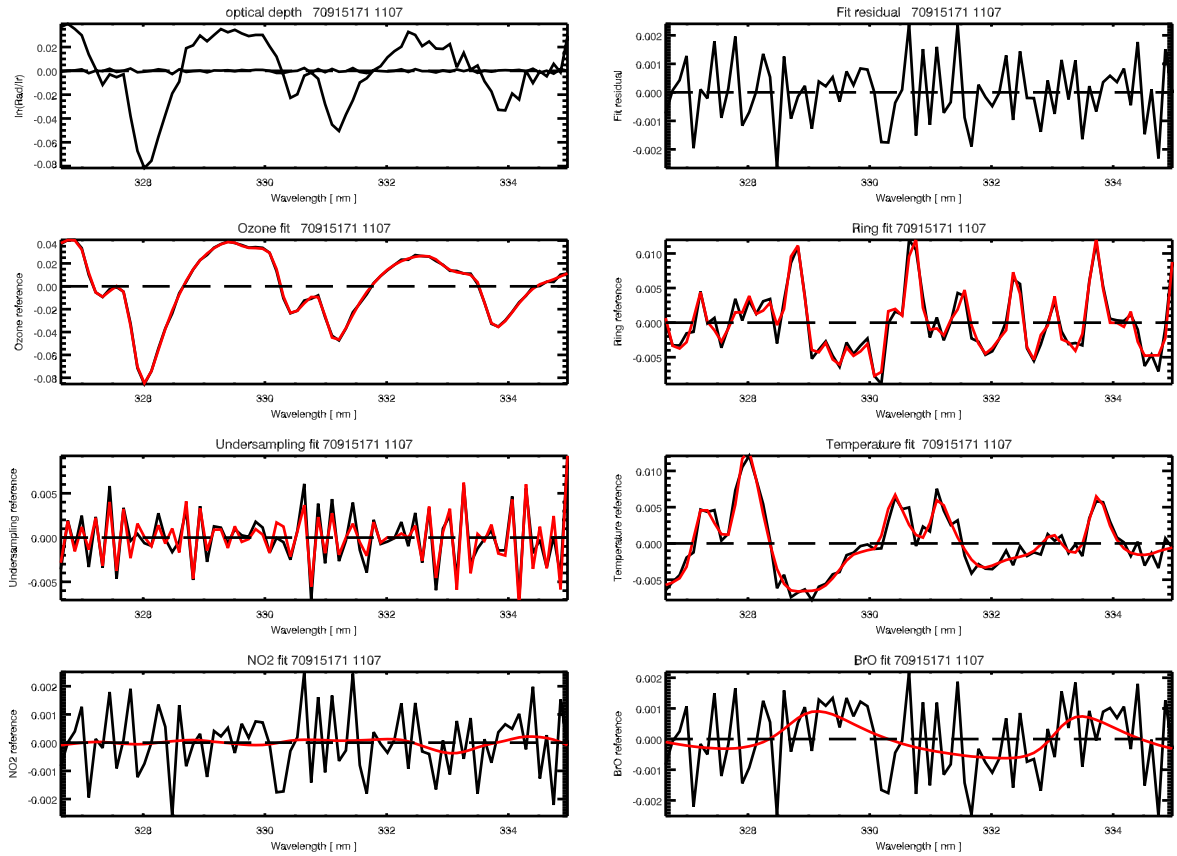

Figure 4.6: *Fit residual of pixel number 1107 (tropics) in GOME orbit 70915171. The GOME observed differential optical depth (left) and fit residual (left and right) are shown in the two top panels. The lower panels show the magnitude of the various terms in the WF-DOAS equation. Red lines show the modeled values and the fit residual has been added to each term (black) to visualize the relative magnitude of the measurement noise. The following terms are shown in the lower panels (from top to bottom and left to right: ozone, Ring, undersampling correction, temperature shift, NO2, and BrO. The fit RMS is on the order of 0.001.*

5 Ring-effect in WF-DOAS

Many ground-based instruments. e.g. zenith-sky spectrometer, and satellite instruments such as GOME and TOMS observe the *filling-in* of solar Fraunhofer lines in the scattered light (Grainger and Ring, 1962). The dominant contribution to this effect is rotational Raman scattering (RRS) on air molecules (Kattawar *et al.*, 1981) and is generally referred to as the Ring effect. Rotational Raman scattering has to be accounted for in ground based zenith-sky measurements (Solomon *et al.*, 1987; Fish and Jones, 1995) and backscatter UV satellite measurements (Joiner *et al.*, 1995; Chance and Spurr, 1997; Vountas *et al.*, 1998) when retrieving trace gas columns from scattered light. The most common procedure is to use the so-called Ring spectrum, which is the optical depth difference of intensities with and without the Ring effect, as an effective absorber in the standard DOAS retrieval (Solomon *et al.*, 1987; Vountas *et al.*, 1998). In the Huggins band the Ring spectrum has the largest contribution to the differential optical depth after ozone itself. This filling-in is usually strongest in those spectral regions where the modulation of intensities with wavelength are largest, for instance around the Ca II h and k Fraunhofer lines near 395 nm (see bottom panel of Fig. 2.1). It is therefore plausible that in regions where ozone absorption contributes to the intensity modulation of scattered light (as in the Huggins band) non-negligible contribution to the molecular *filling-in* by ozone does contribute to errors of several percents in the retrieved total column if not accounted for, as is the case in the current GDP V3.0 (Roozendael *et al.*, 2003).

The change in the so-called Ring spectrum for nadir observations as a function of total ozone (using the corresponding profile shape from TOMS V7 climatology) is demonstrated in Fig. 5.1. The Ring spectra were calculated with SCIATRAN/CDI (Rozanov *et al.*, 1997; Vountas *et al.*, 1998). The variability is largest near the absorption peaks of ozone. The largest contribution to the Raman scattering occurs in the Rayleigh layer near the surface. This explains the weakening of the Ring effect as a function of the effective height as shown in Fig. 5.2. The variation of the Ring effect with altitude has been utilized to retrieve cloud-top-heights from backscattered radiation (Joiner and Bhartia, 1995; de Beek *et al.*, 2001).

5.1 Implementation in WF-DOAS

In order to account for the dependence of the Ring effect on various atmospheric parameters like ozone, altitude, solar zenith angle, and albedo, it was decided to establish a Ring data base corresponding to the atmospheric scenarios defined for the reference intensities and weighting functions. Since the computational speed for Ring calculation is two order of magnitude lower, not all atmospheric conditions were feasible in the Ring calculation. It can be shown, that the line-of-sight dependence of the Ring effect can be accurately treated by proper scaling of the corresponding nadir Ring amplitude as part of the DOAS fitting. The Ring database was limited to nadir viewing, thereby, avoiding the computationally expensive expansion of Fourier components in azimuth direction in the RTM. A total of 37,128 Ring spectra were calculated and are used in WF-DOAS matching the atmospheric scenarios defined for the reference intensities and weighting functions.

In the standard setting for total ozone retrieval several orbits have been analyzed using two different Ring implementations. The first uses a fixed atmospheric scenario from MPI-2D CTM climatology (October 75°N, M. Vountas, personal communication) and varies only with solar zenith angle, the second uses the full Ring

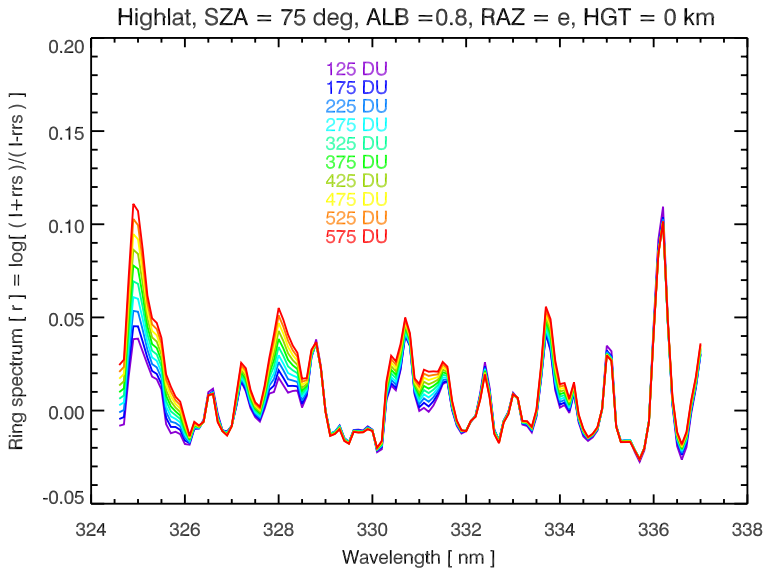

Figure 5.1: *SCIATRAN modeled Ring spectra using the high latitude TOMS V7 ozone profile climatology for different total ozone classes*

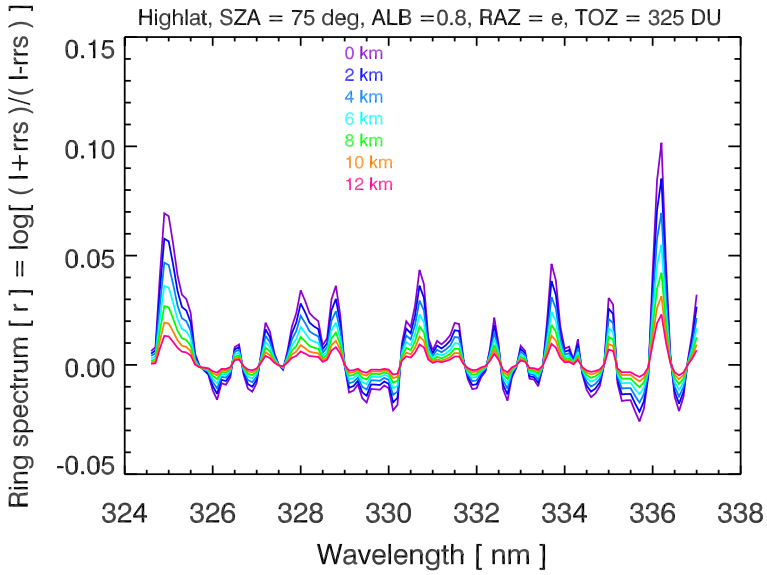

Figure 5.2: *SCIATRAN modeled Ring spectra for a given ozone scenario as a function of altitude/effective height.*

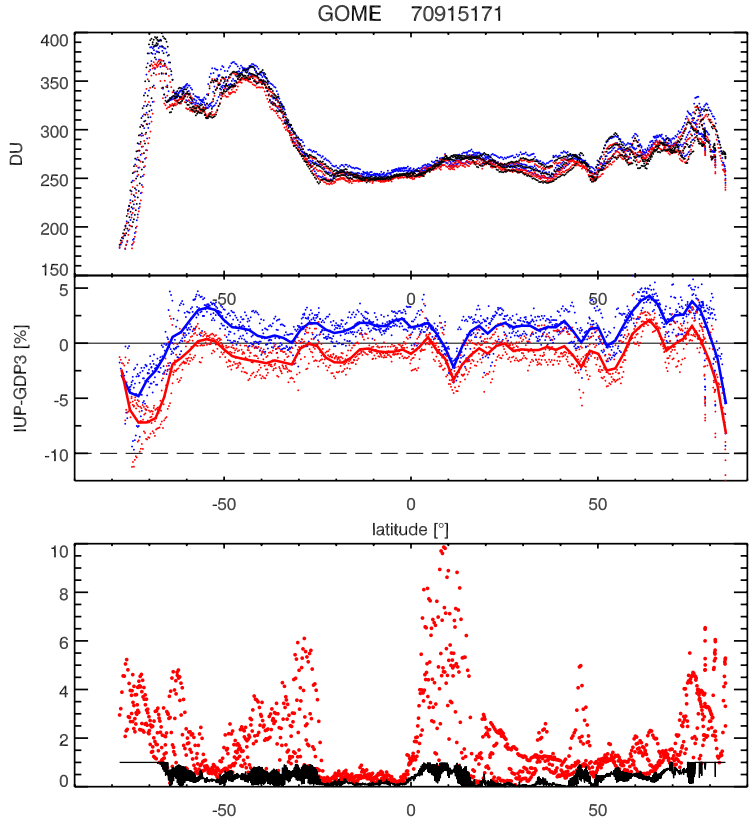

Figure 5.3: *Two different total ozone retrieval by using the full Ring database accounting for molecular filling-in (blue) and by using a Ring spectrum for a fixed atmosphere and varying solar zenith angles (red October 75 N, MPI-2D CTM). Both retrievals were done with the mid-latitude TOMS V7 climatology. Top panel shows total ozone from GDP V3.0 (black), WF-DOAS (blue), and WF-DOAS with fixed-atmosphere-Ring (red). Middle panel shows the differences of both WF-DOAS results to GDP V3.0 in percent. Lines show the corresponding running means through the data. Bottom panel shows the effective height in km (red) and cloud fraction (black) along orbit 70915171.*

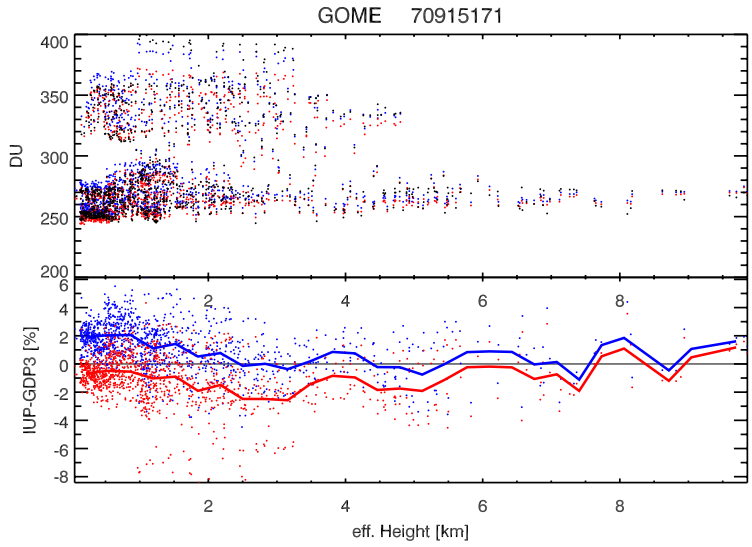

Figure 5.4: *WF-DOAS total ozone retrieval along GOME orbit 70915171 using different Ring implementations (see Fig. 5.3 for explanations). Data are shown here as a function of effective height.*

database properly accounting for the molecular filling–in due to ozone. In Figure 5.3 the total ozone results for both Ring implementations are shown along GOME orbit 70915171 (15th September 1997). The fixed atmospheric scenario in the Ring implementation is about 2% lower than the results using the full Ring database. It should be noted here that the bias may change if a different atmospheric scenario is selected for the fixed atmosphere. Looking at the effective height retrieved along the GOME orbit, it is evident that the differences are smaller above high clouds, for instance in the inner tropical convergence zone (ITCZ), where the effective heights reach a maximum close to 10 km.

If the data are plotted as a function of the retrieved effective height as depicted in Fig. 5.4, it can be concluded that the differences between both Ring implementations get smaller at higher effective heights as theoretically expected from the reduction in the Ring effect due to the hidden Rayleigh layer below the clouds and the diminishing role of molecular filling-in. Figure 5.5 shows the results from 113 orbits from eight selected days distributed over the year 1997 (29th/30th of March, June, September, and December). They confirm the results from the single orbit shown before. The new Ring database yields results which are about one to two percent higher than the GDP V3.0 results (and up to 3% higher than the fixed-atmospheric-scenario Ring).

5.2 Molecular filling-in and ozone temperature

It is evident that the filling-in effect has its largest effects near the ozone peaks (see Fig. 5.1). Both temperature change and molecular filling-in modify the shape of the ozone absorption. In the current GDP V3.0, two O_3 cross-section measured in the laboratory at two temperatures (221 K and 241 K) are fitted to retrieve the slant column amount (Burrows *et al.*, 1999a). The slant column weighted average of the two temperatures can be considered representative of the ozone temperature (Roozendael *et al.*, 2003). The ozone temperature, however, is treated very differently in the WF-DOAS. The temperature shift weighting function is a scalar parameter and yields the change in radiances from a temperature offset applied to the entire T–profile. An effective temperature can be defined by adding the retrieved offset from WF-DOAS to the ozone weighted integrated TOMS V7 temperature profiles. For the GOME orbit (7091517) the effective temperature has been derived and results are depicted in the left panel of Fig. 5.6. Also shown is the retrieved effective temperature from a two temperature slant column fit. Differences of up to 10 K can be noted from the two analyses. The more realistic decrease in the effective temperature by the two temperature fit in the south polar region differs strongly from the WF-DOAS analysis, showing only a very modest decrease.

Repeating the analysis using the fixed–atmosphere Ring implementation show a quite different behavior in the effective temperature (right panel of Fig. 5.6). A lowering in the effective temperature by up to 10 K is observed in the two temperature fit, while the WF-DOAS results show only very small decrease of up to 3 K. The retrieved effective ozone temperature strongly depends on the way how the temperature effect is accounted for in the retrieval and on the proper modeling of the molecular filling–in.

Another interesting effect can be observed when comparing the fit residual root-mean-square sum (RMS) with regard to the different Ring implementations. The new Ring database apparently results in higher fit RMS than the fixed–atmosphere Ring. The new Ring database was calculated at an equidistant wavelength grid (0.1 nm). The Ring spectra, therefore, have to be interpolated to the retrieval grid that is basically determined by the solar

reference used in the fit. Due to the undersampling of the GOME spectra, the retrieval then adds interpolation noise to the fit RMS. The fixed-atmosphere Ring spectrum, however, has been derived at the same GOME sampling grid as the GOME solar reference spectrum used in the Ring calculation and is consequently void of interpolation errors. In the next upgrade the Ring database will be acquired at the GOME sampling grid. For a few selected cases some of the new Ring spectra has been re-calculated using the GOME sampling grid of the solar reference including the Kurucz shift. The fit RMS went slightly below the range observed with the fixed–atmosphere Ring. The reverse is also true if the fixed–atmosphere Ring spectra are interpolated to an equidistant 0.1 nm sampling grid, the fit RMS increases correspondingly. It should be emphasized here that the difference in the fit RMS had no bearing on the retrieved column amounts.

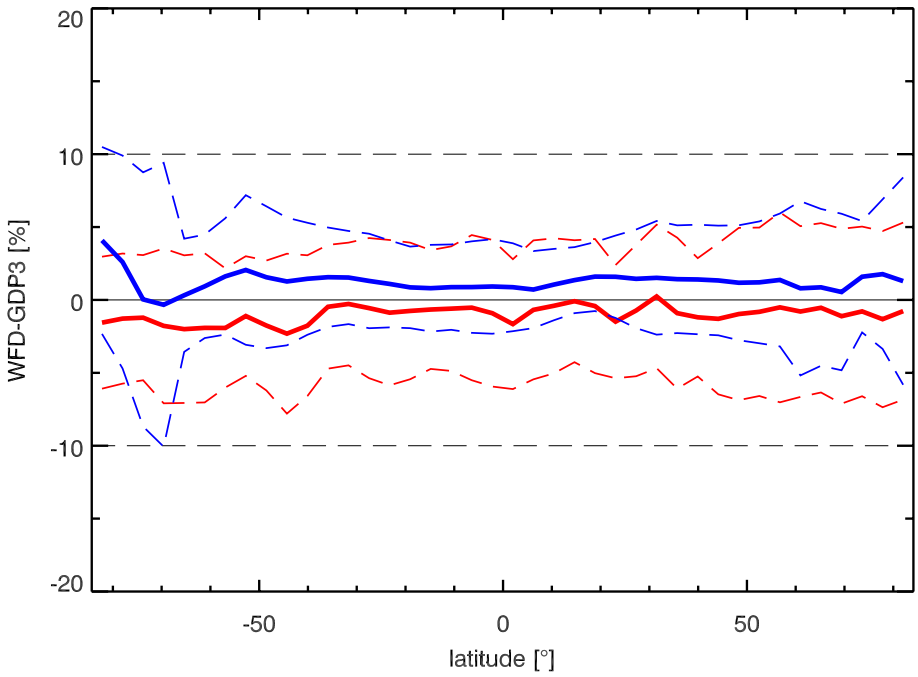

Figure 5.5: *Differences to GDP V3.0 over 113 orbits from eight days distributed over 1997 (29th/30th of March, June, September, and December). Shown are the difference of WF-DOAS with Ring database (blue) and with a fixed atmospheric scenario Ring allowing only variation in solar zenith angle (red). The dashed curves indicate the 2σ standard deviations of the differences.*

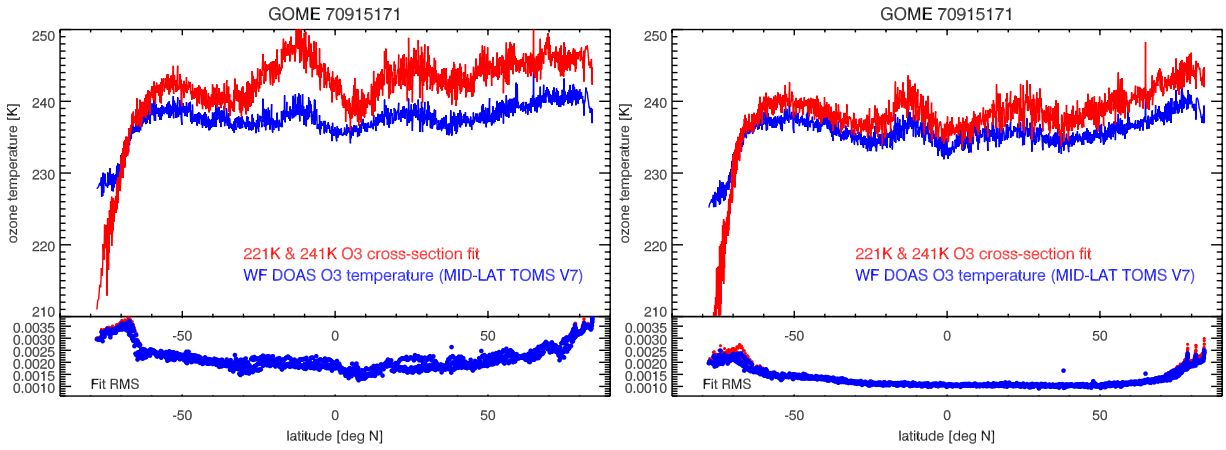

Figure 5.6: *Ozone temperature retrieved from WF-DOAS analysis (blue) and two temperature cross-section fit (red) along orbit 70915171. See text for definition of ozone temperature for both retrievals. Left panel shows results using the new Ring database; right panel shows results using the fixed–atmosphere Ring spectra. In the bottom the RMS of the fit residuals are shown that are basically identical for WF-DOAS and standard DOAS retrieval when using the same Ring implementation.*

6 A-priori Ozone Climatology in WF-DOAS

In the WF-DOAS retrieval the total ozone dependent TOMS V7 ozone profile shape climatology (Wellemeyer *et al.*, 1997) is used as a-priori information on the profile shape required to calculate weighting functions and reference radiance spectra. This climatology is divided into three latitude bands, i.e. tropics (0°–30°), mid-latitudes (30°–60°), and high latitudes (60°–90°) and between six (tropics) and ten ozone classes (mid- and high latitudes) spanning a range between 125 DU to 575 DU in steps of 50 DU. There is no distinction between hemispheres. In this section the sensitivity of the climatology on the GOME WF-DOAS retrieval is investigated.

Figure 6.1 shows the different ozone results along orbit 70915171 using a-priori ozone profiles defined for the three latitude bands (LOW_LAT, MID_LAT, HIGH_LAT). For most part of the orbit the three climatology yield similar results apart from a small bias ($+1\%$ for LOW_LAT and -2% for HIGH_LAT with respect to the MID_LAT analysis.) At higher latitudes (high SZA) the curves appear divergent. The mid-latitude and low latitude results decrease relative to GDP V3.0, while the results with high latitude profiles rather increase towards high latitudes. The proximity of the low and mid-latitude profile results can be explained by the fact that the low ozone profiles in these region are associated with high tropopause (characteristic for tropical and sub-tropical airmasses that can extend well into the mid-latitudes, "ozone mini hole"), whereas the high latitude profiles with low total ozone correspond to ozone hole profiles (low tropopause and depleted ozone near 20 km altitude). The solar zenith angle dependence for the three regions are shown in Fig. 6.2. The Umkehr effect becomes evident at solar zenith angles above 75° SZA.

Figure 6.3 shows the differences to GDP V3.0 results averaged over 113 orbits from eight days distributed over 1997 (29th/30rd of March, June, September, and December). Results using LOW_LAT profiles are about 1% above MID_LAT results and about 2% above HIGH_LAT results, the latter being closest to GDP V3.0, if applied to all latitudes. As a function of effective altitude the differences to GDP V3.0 increases by up to 2% above 8 km effective height. In GDP V3.0 the cloud-top-height is determined from an empirical formula derived from a cloud climatology and is not retrieved from the GOME radiances itself. In this regard the WF-DOAS that includes the retrieved cloud-top-height (effective height) and effective albedo represents an improvement over GDP V3.0.

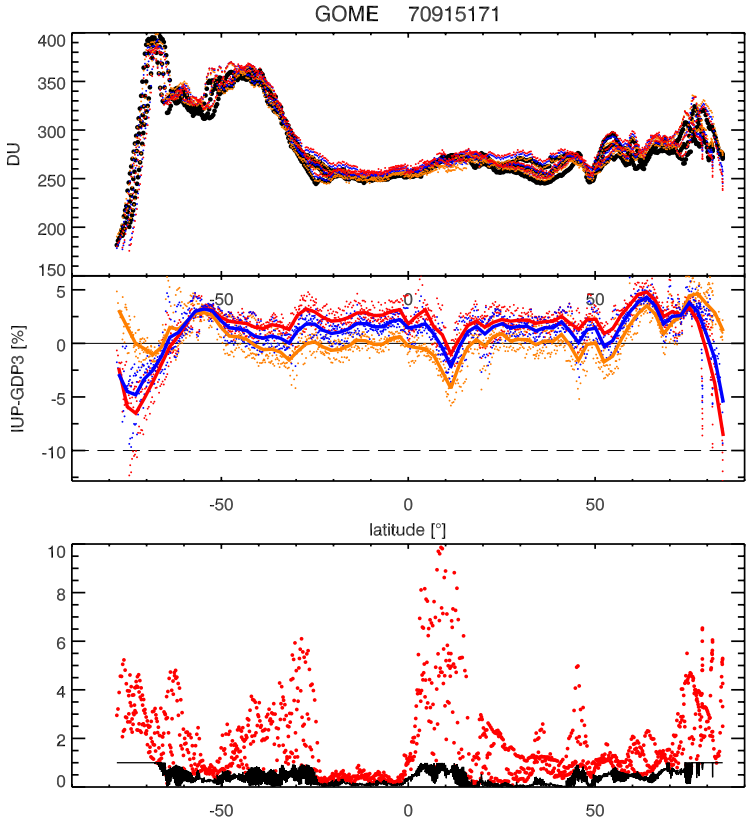

Figure 6.1: *Total ozone results along the GOME orbit 70915171. Different results from using the LOW_LAT (red), MID_LAT (blue), and HIGH_LAT (orange) TOMS V7 profiles in WF-DOAS are shown for the entire orbit 70915171. In the top panel the GDP V3.0 data (black) are also shown. Middle panels shows the differences to GDP V3.0 in percent. Bottom panel shows the retrieved effective altitude in km (red) and the retrieved cloud fraction (black).*

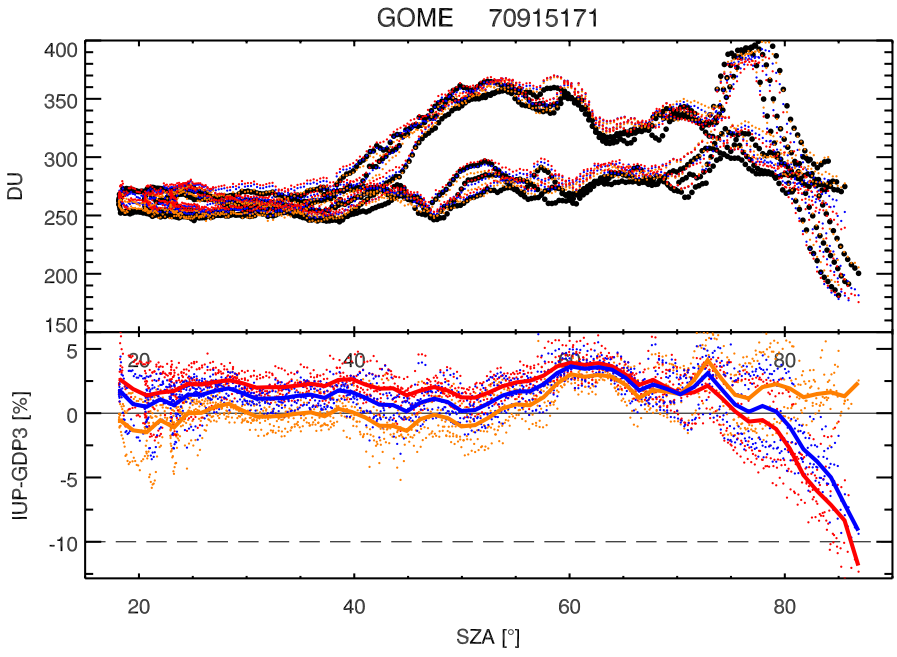

Figure 6.2: *Same as Fig. 6.1 but plotted as a function of solar zenith angle.*

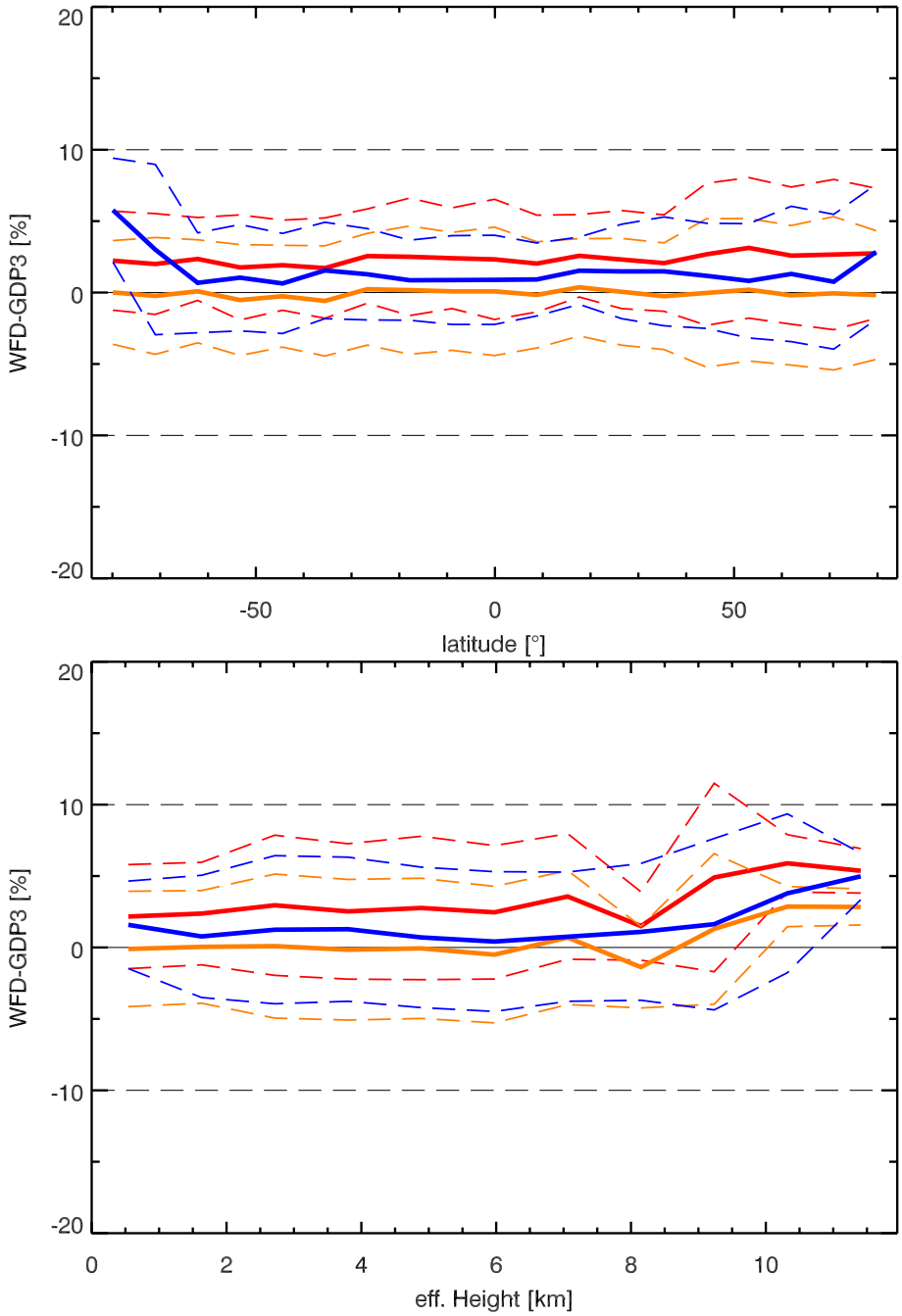

Figure 6.3: *Differences from WF-DOAS results with different zonal profiles with respect to GDP V3.0 averaged over 113 orbits from eight days distributed over 1997 (29th/30rd of March, June, September, and December). Results using the LOW_LAT, MID_LAT, and HIGH_LAT TOMS V7 profiles in WF-DOAS are shown in red, blue, and orange, respectively. The dashed lines show the $\pm 2\sigma$ lines of the observed differences. Top panel shows the results as a function of latitude,; the bottom panel as a function of retrieved effective altitude.*

7 Selected Case Studies

7.1 Enhanced aerosol loading

Anthropogenic and natural aerosols in the atmosphere change the radiative properties by scattering and absorption of solar irradiance. As the WF-DOAS reference spectra look-up-table does not consider different aerosol scenarios and types, errors in fitted ozone vertical column may arise for scenes with enhanced aerosol loading.

Aerosols which only scatter the light (single scattering albedo ω_0 is close to one) can be accounted for by our concept of using the Lambertian equivalent reflectivity instead of surface albedo as input for ozone retrieval. This effective reflectivity at 377.6 nm accounts for scattering by clouds, aerosols, and the surface as well as Rayleigh scattering. Errors are expected to be small in this case. On the other hand, absorbing aerosols are not corrected for with this method.

We have computed some synthetic test spectra for different aerosol types to estimate the ozone vertical column error. Solar zenith angle was 60°, and we selected an ozone amount of 325 DU ($= 879.53 \cdot 10^{16}$ molec/cm^2) for a low latitude profile from TOMS V7. The LOWTRAN aerosol model (Shettle and Fenn, 1976, 1979) was used which allows aerosol types rural, urban, tropospheric, and maritime in the boundary layer and troposphere. For the stratosphere, a background profile, moderate, high or extreme volcanic profiles can be selected. Besides there is a distinction between season (spring/summer or fall/winter) and different visibilities are possible (2, 5, 10, 23 or 50 km).

Five test spectra with enhanced aerosol loading (visibility of 2 km) and one scenario with low aerosol amount (here called standard scenario, visibility of 23 km) were calculated for the wavelength region of our fit window. Additionally, intensities from 376–378 nm were computed for LER retrieval, which was performed for each spectrum before the ozone fitting procedure. Two surface albedo values were selected (0.05 and 0.2).

Figure 7.1 shows the intensity ratio with and without aerosol for the different aerosol types (in brackets: retrieved LER). The so-called standard scenario is maritime aerosol at 23 km visibility. Except for urban and volcanic aerosol (absorbing aerosols), TOA reflectivity is enhanced compared to an atmosphere without aerosol.

Table 7.1 contains retrieved LER and fit results for all scenarios. Third and fourth column indicate fit results and errors when LER is used as effective albedo, and sixth and seventh column contain the same for surface albedo (0.05 and 0.2) as input. Errors are below 0.3% for those types where reflection prevails (non-absorbing), if scene reflectivity is used as part of the rerieval. The LER is able to account for this enhanced reflectivity and can be regarded as a first order correction. Only for absorbing urban aerosol the error becomes higher. If the surface albedo is used as input, errors can be as large as 3% for non-absorbing aerosols and the lower albedo value (0.05). The error figures for absorbing aerosols is similar to the the retrieval incdluding LER and can lead to systematic errors of -2% to -1%.

To summarise, the error due to non-absorbing aerosols is less than 0.3% and for absorbing aerosols the ozone column may be underestimated by 1% if visibility is reduced to 2 km.

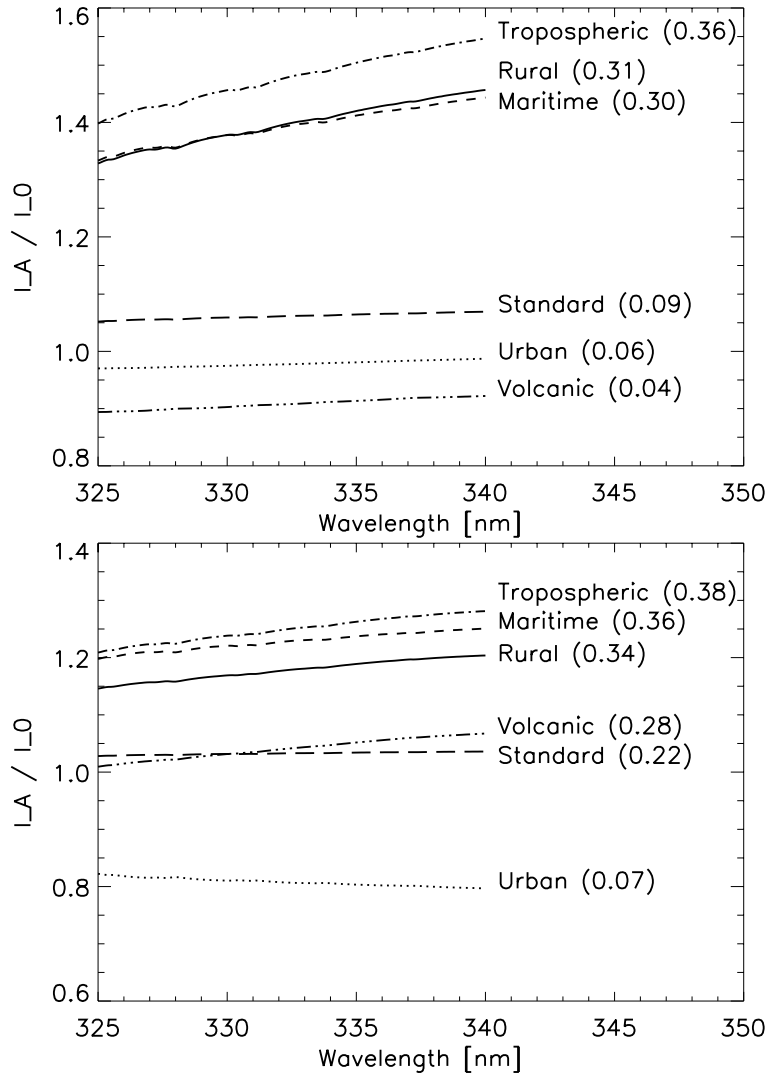

Figure 7.1: *Ratio of radiance with different aerosol types at 2 km visibility, I_A, to radiance without aerosol (I_O). Top: surface albedo $a_o = 0.05$ and bottom $a_o = 0.2$. In brackets: the retrieved LER.*

Table 7.1: *Fit results and errors for different aerosol scenarios. Top half: surface albedo, a_o=0.05, and bottom half: surface albedo, a_o=0.2. τ is aerosol optical depth and ω_o the surface single scatter albedo at 337.1 nm. Error figures to the left are for retrieval with LER as effective albedo and right for retrieval with surface albedo as effective albedo.*

Aerosol Type	τ @337.1 nm	ω_o	LER [-]	O_3 [10^{16} molec/cm^2]	Error [%]	a_o [-]	O_3 [10^{16} molec/cm^2]	Error [%]
Standard $a_o = 0.05$	0.38	0.99	0.09	878.02	-0.17	0.05	881.50	0.22
Maritime	3.4	0.99	0.30	881.40	0.21	0.05	901.50	2.50
Tropospheric	5.0	0.96	0.36	878.96	-0.06	0.05	903.25	2.70
Rural	4.8	0.94	0.31	878.42	-0.13	0.05	899.19	2.24
Volcanic	0.6	0.81	0.04	870.14	-1.10	0.05	869.23	-1.17
Urban	4.6	0.66	0.06	871.95	-0.86	0.05	872.84	-0.76
Standard $a_o = 0.2$	0.38	0.99	0.22	880.09	0.06	0.2	881.89	0.27
Maritime	3.4	0.99	0.36	882.06	0.29	0.2	894.57	1.71
Tropospheric	5.0	0.96	0.38	879.56	0.00	0.2	893.31	1.57
Rural	4.8	0.94	0.34	878.68	-0.10	0.2	889.10	1.09
Volcanic	0.6	0.81	0.28	877.37	-0.25	0.2	884.11	0.52
Urban	4.6	0.66	0.07	871.32	-0.93	0.2	861.68	-2.03

7.2 Tropics

Total ozone column in the tropics shows lower variability as compared to the higher latitudes. Little dependence of the tropical ozone on effective altitude, albedo, or cloud cover should be observed, if the cloud correction, albedo retrieval, as well as the GVC corrections are properly carried out. In order to test this, a selected region in the eastern Pacific (20°N to 20°S and 120°W to 180°W) from the period 16–18 September 1997 (about 2400 GOME pixels) were analyzed. Figure 7.2 shows the results as a function of the retrieved effective altitude, cloud fraction, and effective albedo. In all cases the correlation is below 0.15.

7.3 Mountains

In this Section it is demonstrated that the algorithm delivers reasonable results for GOME pixels covering high mountains such as the Andes and Himalaya. The higher the ground altitude the less ozone should be retrieved. Figure 7.3 (Andes) and Figure 7.4 (Himalaya) show total ozone columns from September 1997 over the Andes (0° - 40° S and 60° W - 85° W), and from June 1997 over the Himalaya (25° N - 40° N and 70° E - 100° E). Only pixels with cloud fraction less than 0.2 were included. Figures 7.3 and 7.4 (top panel) show total ozone as as function of altitude. It decreases with increasing height. Correlation coefficient is $\rho = -0.38$ for Himalaya pixels and $\rho = -0.25$ for the Andes. Middle and bottom panel of Figure 7.4 show in addition total ozone and ground altitude as a function of latitude. Lower ozone is observed above the Himalaya. Ozone values above 300 DU were only observed at low surface altitude close to the Andes and north of the Himalaya range that may indicate enhanced tropospheric ozone.

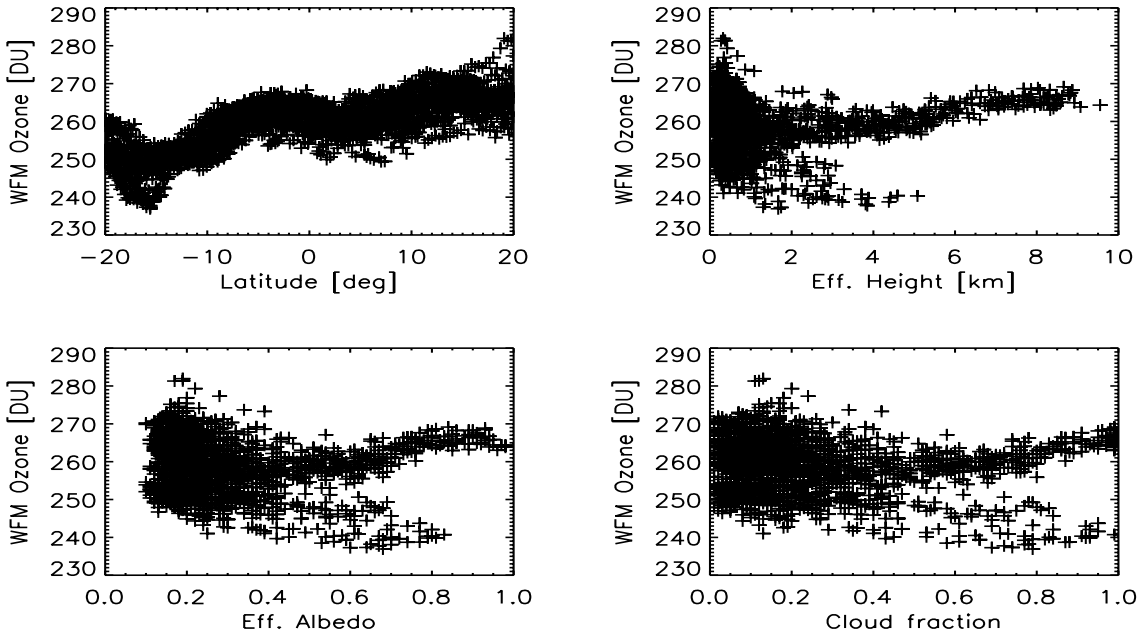

Figure 7.2: *Total ozone in the tropics as a function of latitude (upper left), effective altitude (upper right), effective albedo (bottom left), and cloud fraction (bottom right). 2400 pixels from eastern Pacific during the period 16–18 September 1997 were taken into account.*

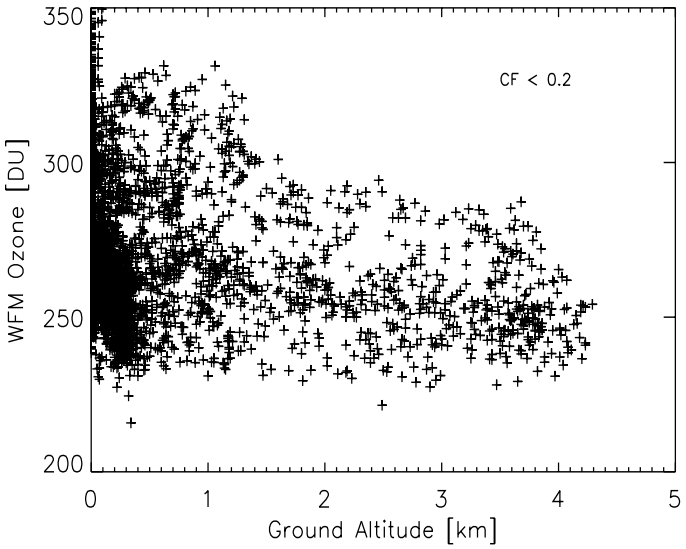

Figure 7.3: *Influence of ground altitude on ozone retrieval in Andes region. All GOME data from September 1997 with cloud fraction less than 0.2 are shown.*

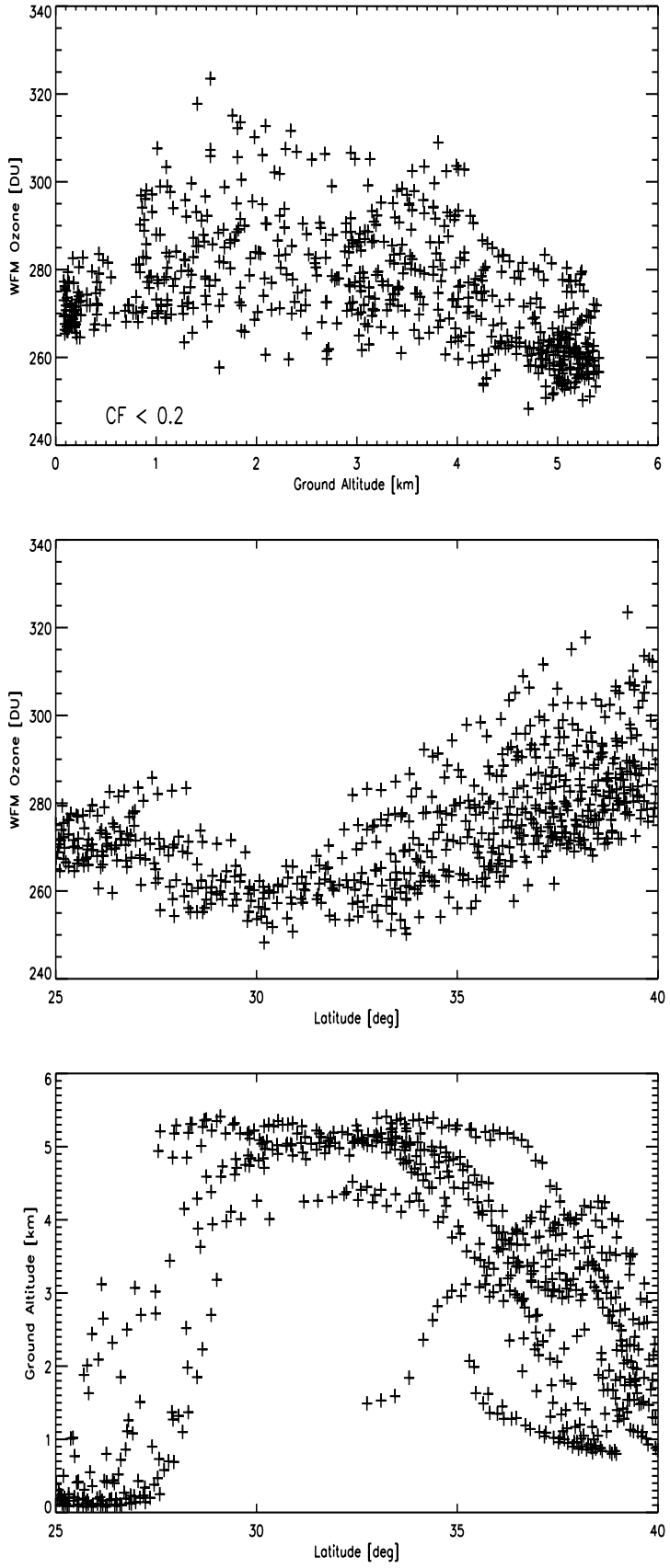

Figure 7.4: *Influence of ground altitude on ozone retrieval in Himalaya region. GOME data from June 1997 with cloud fraction less than 0.2 are shown.*

8 Error Analysis

In this Section the various error sources are summarized that contribute to the overall error of retrieved ozone column. Most of the errors have been investigated as part of this study. The list of errors has been complemented from other investigations that were available at the time of this report. From all this information a global error budget has been derived.

8.1 A-priori Errors

8.1.1 Ozone and temperature profile

The influence of differences between true ozone and temperature profiles and those profiles used in the reference spectra has been investigated. 12 radiance spectra were computed using different ozone and temperature profiles for high latitudes (January to December, 65°N) taken from 2D model calculations performed at the Max-Planck-Institute (MPI) in Mainz, Germany (C. Brühl, personal communication, 1992). All profiles were scaled to 325 DU. Solar zenith angles varied between 50° and 80° and albedo was 0.05. The reference spectra used in the fitting were calculated with only one ozone and temperature profile taken from high latitude TOMS V7 climatology. A comparison of temperature profiles from MPI and TOMS are shown exemplarily in Figure 8.1 Large deviations occur which may may reach 20 K between 35 and 40 km. Fit results for all 12 synthetic spectra are shown in the left panel of Fig. 8.2. The errors are generally below 5%. Largest errors occur in January and December when solar zenith angle is 80°. If the temperature weighting function is not included in the fit, deviations of up to 12% between retrieved columns and correct columns are obtained. Figure 8.2 (right panel) shows a comparison between the temperature from MPI climatology at maximum ozone concentration (21 km) and the retrieved temperature. The algorithm is able to reproduce the temperature with errors smaller than 2% if SZA is below 70°. Additionally a correlation to the differences in ozone column is found. Overestimation of ozone leads to underestimation of temperature and vice versa. This is explained by correlations between temperature and ozone weighting functions which have the same sign.

As discussed in Section 6 GOME analysis with a-priori profiles from different climatic regions (low-, mid-, and high-latitudes) indicate potential systematic errors on the range of 2%. That error increases to 5% at high SZA.

8.1.2 Effective albedo

The influence of an error in the effective albedo input on the retrieved column of ozone has been investigated using two synthetic spectra, both calculated with an albedo of 0.7 and an ozone of $736.5 \cdot 10^{16}$ molec/cm^2. For the retrieval we assumed an albedo of 0.6, 0.8 and 0.9. The retrieval errors are listed in Table 8.1 and they can reach up to 3%.

8.1.3 Effective height

From Figure 4.1 (Section 4.2) a one percent decrease in the column amouts per km error in the effective height can be concluded. A potential 1% error (corresponding to 1 km error in effective height) appears realistic taking

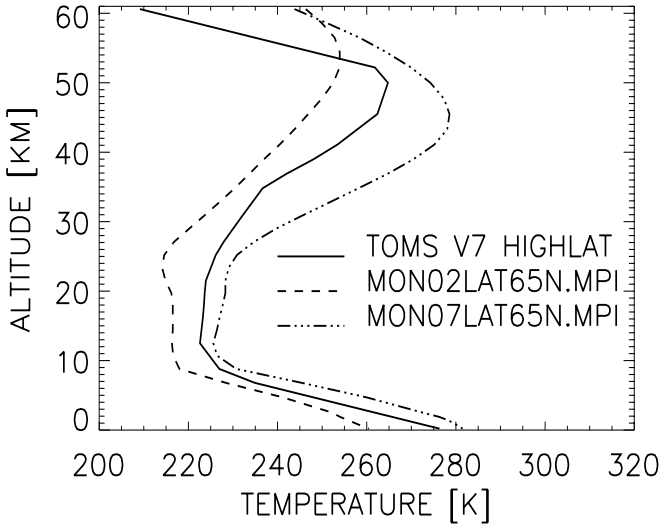

Figure 8.1: *Three temperature profiles. Solid line: TOMS V7 high latitude (325 DU), dashed line: MPI 2D CTM profile (February, 65° N) and dot-dashed line: MPI 2D profile (July, 65° N), both scaled to 325 DU.*

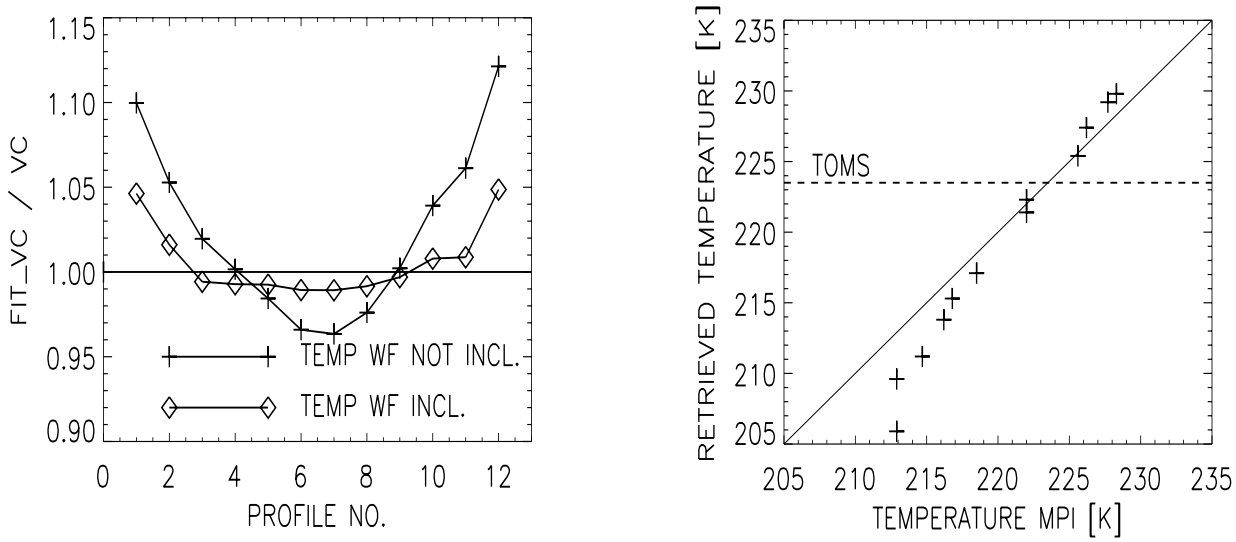

Figure 8.2: *Retrieval results with incorrect ozone and temperature profile input. Left: Ratio of fitted vertical column to correct vertical column for 12 different MPI 2D profiles (all 65° N) from January (No. 1) to December (No. 12). Crosses denote results without temperature weighting function included in the fit, and rhombs denote those results with temperature weighting function included in the fit as normally done in WF-DOAS. Right: Retrieved temperature at 21 km altitude against correct temperature from MPI input profile.*

also into account the unknown error contribution from the simplifying assumptions made to derive the effective height.

8.2 Look-up-table interpolation errors

- **Effective height**
  Our look-up-table contains seven altitude values from 0-12 km in 2 km steps. We obtained an estimation for the error which occurs due to linear interpolation between reference spectra using synthetic test spectra calculated for 1, 3, $\cdots$, 11 km, three solar zenith angles (45°, 75° and 89°) and two albedos (0.02 and 0.8). Vertical column error is below 0.25% in all cases.

- **Albedo**
  The albedo spacing in our look-up-table is less than or equals 0.2. Maximum error in ozone column due to interpolation is about 0.3% for $SZA = 45°$ and 0.1% for $SZA = 75°$.

- **Relative azimuth angle**
  The error due to linear interpolation between two azimuth angles is below 0.05%. This was based upon anlysis using synthetic spectra at different solar zenith angles.

- **Solar zenith angle**
  Between two solar zenith angles of our look-up-table no linear interpolation is performed. Studies have shown that for large angles beyond 70° the accuracy is not sufficient. Errors may reach a few percent. Therefore, we fit Chebyshev polynomials to radiances and weighting functions as a function of solar zenith angle. These polynomial coefficients are stored in the database. The error that remains by using 22 terms in the expansion is about 0.2% at 89° SZA and -0.4 % at 90°. The error is negligible for smaller solar zenith angles.

  Figure 8.3 denotes the ratio of interpolated radiance to exact radiance as a function of solar zenith angle for three interpolation schemes, linear interpolation, twelve, and 22 Chebyshev polynomial coefficients. Smallest differences occur when 22 coefficients are used, and largest if linearly interpolated.

- **Line-of-sight**
  In order to find a representative reference spectrum for a GOME pixel (east, nadir, west) instead of a highly resolved scan, we compute three spectra per pixel for different LOS (for a nominal pixel size of 320 km acrooss track and 40 km along track). Using the weighted average as described in Section 3.2.2, the vertical column error is below 0.02% (see Fig. 8.4, dotted line). We also tested other schemes to find a representative spectrum (e.g. average after the fitting of three line-of-sight angles in a given GOME pixel), but vertical column errors rather increased (Fig. 8.4 solid line, dashed line and dot-dashed line).

- **Ozone**
  Ozone spacing in our reference spectra look-up-table is 50 DU. The error in vertical column which is obtained for GOME spectra between two grid points is about 0.1% below 80° SZA and 1.5% beyond 80°.

Table 8.1: *Ozone retrieval error due to albedo error*

Albedo input	O_3 column [10^{16} molec/cm^2]	Rel. Error [%]
$SZA = 55°$		
0.6	746.4	1.3
0.8	726.5	-1.4
0.9	716.0	-2.8
$SZA = 85°$		
0.6	744.3	1.1
0.8	728.8	-1.0
0.9	720.8	-2.1

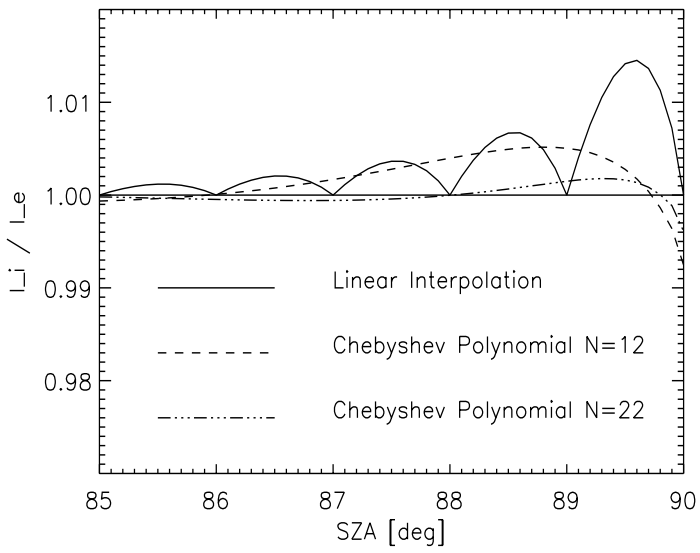

Figure 8.3: *Interpolation error versus solar zenith angle for three different interpolation schemes: linear interpolation (solid line), 12 Chebyshev coefficients (dashed line) and 22 coefficients (dot-dashed line).*

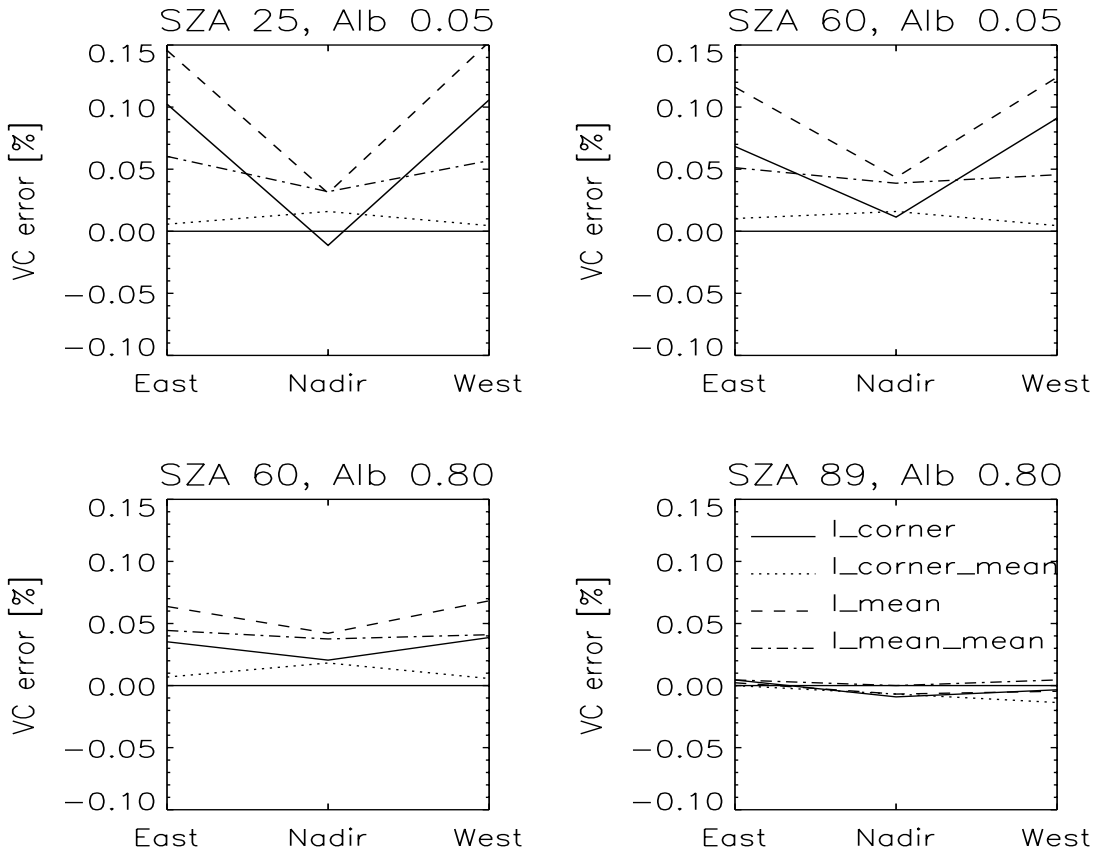

Figure 8.4: *Vertical column errors due to one representative reference spectrum for one pixel instead of a highly resolved scan. Different panels for different solar zenith angles and albedos. Solid line: LOS for pixel corners and center, average after fitting. Dotted line: LOS for pixel corners and center, average before fitting. Dashed line: LOS for pixel center and two intermediate angles, average after fitting. Dot-dashed line: LOS for pixel center and two intermediate angles, average before fitting.*

Table 8.2: *GVC Error for four GOME orbits from 16th March, 18th June, 15th September and 16th December 1997.*

Orbit		70316131	70618016	70915171	71216140
Mean percentage difference	[%]	20	25	15	15
Mean absolute difference	[DU]	0.4	0.4	0.5	0.4
Difference / Total ozone	[%]	0.13	0.15	0.15	0.12

8.3 Ghost vertical column error

FRESCO provides error estimates for cloud fraction and cloud-top-height. They are used to investigate the influence on ghost vertical column and on total ozone. Maximum and minimum ghost column were calculated as follows

$$GVC_{max} = (f + \Delta f) \cdot \int_{p_o}^{p(h_{\mathsf{cld}}) - \Delta p(h_{\mathsf{cld}})} O_3(p)\, dp \tag{8.1}$$

$$GVC_{min} = (f - \Delta f) \cdot \int_{p_o}^{p(h_{\mathsf{cld}}) + \Delta p(h_{\mathsf{cld}})} O_3(p)\, dp, \tag{8.2}$$

where f is cloud fraction and Δf its error and $p(h_{\mathsf{cld}})$ is cloud-top-pressure and $\Delta p(h_{\mathsf{cld}})$ its error. Four orbits from 1997 were evaluated and results are summarized in Table 8.2. Figure 8.5 shows absolute and relative errors as function of latitude. The error due to FRESCO retriveal is well below 0.2%, however, the error due to the simplifying assumptions of clouds as reflecting surface may be more significant.

8.4 Fitting window

The correlation between ozone and temperature weighting function was an important criterion for the fitting window selection. In Section 3.2.5 it has been pointed out that correlation increases with decreasing window width.

Not only window width but also the start wavelength has an influence on this correlation. Fig. 8.6 shows the correlation coefficient as a function of both window width (varying from 3 to 8 nm) and starting wavelength (top panel). Large negative correlation coefficients can be found for small fit windows and the wider the fit window the smaller the correlation gets. Moreover, the correlation increases when start wavelength is close to a minimum in ozone cross section (which is depicted in the bottom panel for comparison). The lowest absolute correlation coefficient ($\rho = -0.46$) was found for the fit window 328.4–334.9 nm. It is very similar to the OMI fitting window 331.6–336.6 nm (R. van Oss, personal communication) that has a correlation coefficient of $\rho = -0.45$.

About three hundred GOME overpasses over Hradec Kralove, Czech Republic, have been analysed using this window setting. Since the window width is smaller than the window used in V1.0 (326.6–335 nm) only a quadratic polynomial was permitted in the iterative fit. The differences were well below 0.1% with respect to V1.0. For both windows the temperature shift weighting function was included in the fitting.

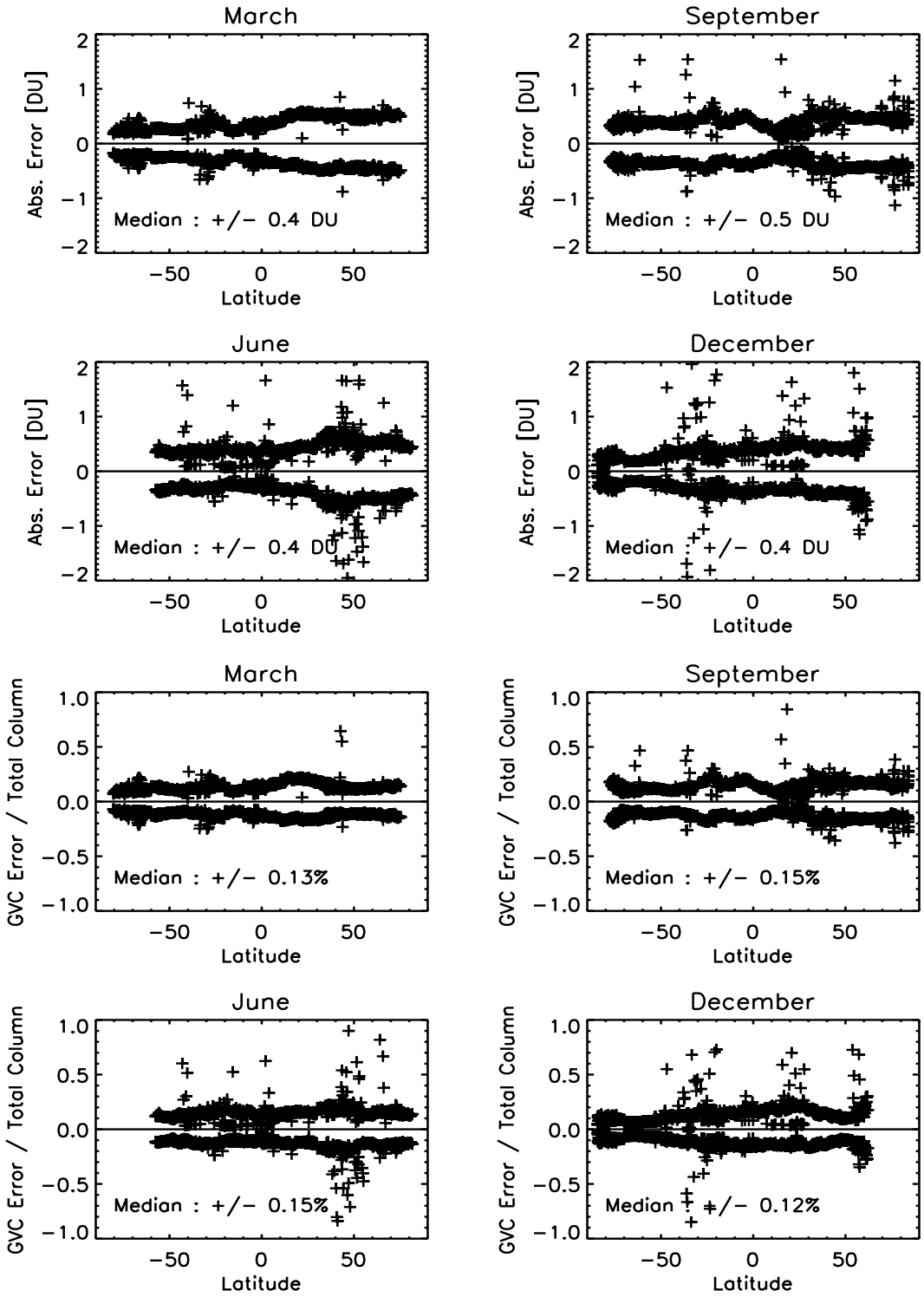

Figure 8.5: *Ghost vertical column errors as function of latitude. Top: Absolute difference and bottom: percentage error with respect to total ozone.*

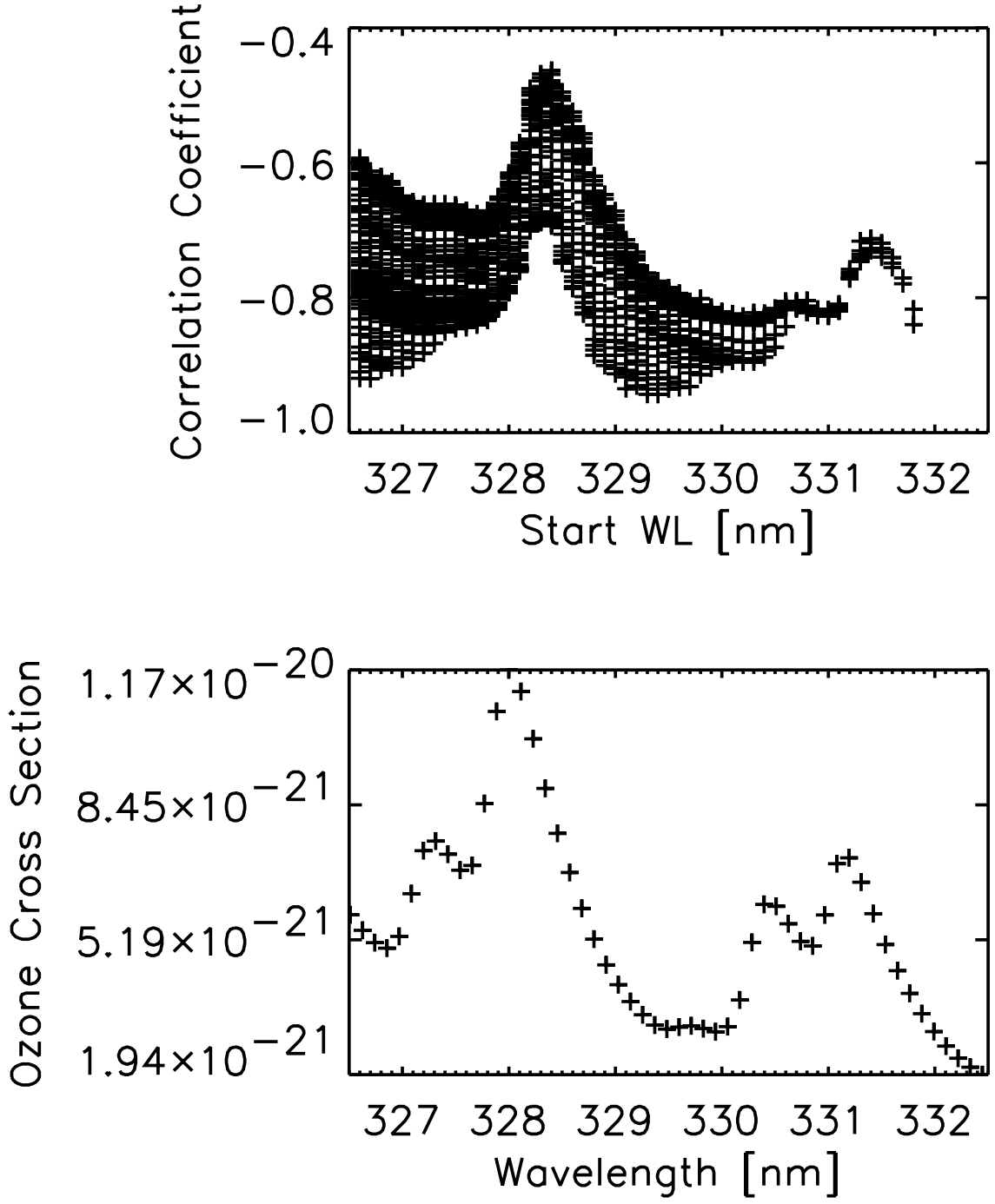

Figure 8.6: *Top: Correlation between ozone and temperature weighting function as a function of start wavelength and window width. Large negative coefficients occur for smaller fit windows. Bottom: GOME FM98 ozone cross section (241 K).*

8.5 Other error sources

- **Pseudo-spherical approximation**
  The relative total ozone column error, which remains when the pseudo-spherical approximation instead of full-spherical radiative transfer modelling is used, is about 0.3%. This is the case for solar zenith angle and line-of-sight at the ground level is used in the pseudo-spherical approximation. The absolute radiance error for the pseudospherical SCIATRAN/CDI is below 2% for SZA $\leq 92\,^{\circ}$ (Rozanov *et al.*, 1997).

- **Fraunhofer fit**
  The Fraunhofer fit changes the ozone VCD by up to +2% as shown in Figure 3.5.

- **ozone filling-in in Ring**
  Differences of up to 3% can be obtained when compared to retrievals using Ring spectra determiend for a fixed ozone column. This error figure agrees qualitatively with results from the GDP V3.0 Implementation document (GDP V3 VALREPORT, 2002; Roozendael *et al.*, 2003). The error strongly depends on the atmospheric conditons (cloudiness and effective height) as discussed in Section 5

- I_o**-effect**
  This effect has been investigated in a few cases. In this study a difference spectrum, with and without I_o correction was used, since the reference spectra and WF were calculated using the original cross-section spectra. A reduction in fitting RMS of up to 10% were observed and ozone columns were reduced by about 0.2% confirming the results reported in GDP V3 VALREPORT (2002). It bshould be noted here that it correlates strongly with the retrieved temperature shift.

- **Errors due to aerosols**
  In Section 7.1 the error due to neglecting high aerosol loading in the radiative transfer has been discussed by using simulations of various scenarious covering non-absorbing and absorbing aerosols. For non-absorbing aerosols the ozone column error is well below 0.3% (2 km visibility) if the effective albedo is measured and used in the retrieval. Enanced aerosols leads to to higher scene albedo and represents a first order aerosol correction to the ozone column. In the presence of non-absorbing aerosols the retrieved ozone column may be underestimated by about 1% (urban aerosols, 2 km visibility).

8.6 Errors from external studies

In a recent GOME-2 Error Study Assessment (Kerridge *et al.*, 2002; de Beek *et al.*, 2003) several error sources were investigated that also apply for GOME/ERS. Both GOME-1 and GOME-2 are nearly identical in optical design, so that some of the error investigated in that study can be also assigned to GOME-1. These were mainly errors related to polarisation correction, ground Al diffuser plate, and signal-to-noise.

The theoretical accuracy due to signal-to-noise in GOME Channel 2 is for ozone in the UV window about 0.3%, and 3% in the Chappuis band. Broad-band Si photo diodes measure the polarisation state of the atmopsheric light passing the spectrometer (Burrows *et al.*, 1999b). The band width approximately matches the width of the

science channels covering several tens of nanometer. These measurements are used to apply a correction to the observed radiances to account for both intrument related and atmospheric polarisation effects. Due to lack of spectral resolution in the PMD (polarisation measurement devices) the fine polarisation structures observed in the Huggins band cannot be resolved and leads to error in the polarisation correction scheme. The polarisation correction error can cause an error of 0.5%, in selected cases of up to 1% for total ozone in the UV window (Kerridge *et al.*, 2002; de Beek *et al.*, 2003).

It has been found that the ground Al diffuser plate exhibits differential structures (interference pattern) that varies with solar incident angle and produces seasonal signatures in time series of minor trace gas columns. Errors of up to 100% have been identified for BrO and NO_2 (Richter and Wagner, 2001). Due to the strong absorption of ozone the error is here significantly smaller. Bramstedt *et al.* (2003) investigated the change in total column for different solar incident angles as GOME passively tracks the sun once each day. He derived a O_3 column variation of 0.3%, that can be regarded as an approximate estimate of the diffuser error for ozone.

The error due to the use of Bass-Paur cross-sections, which are commonly used in ozone retrieval from ground-based Brewer and Dobson spectrometers, has been investigated by Roozendael *et al.* (2003) and they cite an error of $\pm 2\%$.

8.7 Global error budget

Table 8.3 is a summary of all errors which were identified for WF-DOAS thus far. Some other errors that were already identified for earlier GOME retrieval schemes and/or from other studies, e.g. selection of cross-sections, differential structures from diffuser plate, and polarisation correction error remain valid for WF-DOAS and are also listed for completeness (Kerridge *et al.*, 2002; GDP V3 VALREPORT, 2002; de Beek *et al.*, 2003). It should be also noted that errors cited here can be larger at high solar zenith angles if not explicitly stated.

Propagation of all error cited in Table 8.3 except for the error impacts when omitted in WF-DOAS (last block in Table 8.3) one arrives at a pecision of the WF-DOAS total ozone retrieval on the order of 3%. The error increases at solar zenith angles above 80° to at least 5%. The largest contribution to the overall error comes from the a-priori errors associated with the use of climatology and simplyfing assumptions made in the derivation of effective parameters. Most of these errors are systematic errors and are, therefore, not random.

Table 8.3: *Summary of all WF-DOAS related error sources applying for total ozone.*

Error Source	**Percent Error**
A priori Errors	
profile shape: O_3 and T	1% below 80°SZA 5% beyond 80°SZA
profile shape (climate zone)	2% below 80°SZA 5% beyond 80°SZA
effective albedo	$\sim$ 1.5%
effective height	1%
LUT Interpolation error	
albedo	0.30%
altitude	0.25%
relative Azimuth Angle	0.05%
line-of-sight	0.02%
solar Zenith Angle	0.2% below 89°SZA
ozone	0.1% below 80°SZA 1.5% beyond 80°SZA
Other errors	
enhanced absorbing aerosol loading	-1%
polarisation correction error	0.5% (1)
enhanced non-absorbing aerosol loading	$<$0.3%
ground Al diffuser plate error	$\sim$0.3% (1)
signal-to-noise ratio	0.3% (1)
pseudo-spherical approximation	0.3% (1)
GVC error w.r.t. GVC	25%
GVC error w.r.t total ozone	0.15%
Error impact if not applied in WF-DOAS	
Fraunhofer fit (Kurucz)	$\sim$+2%
Bass-Paur vs. GOME FM98 O_3 cross-section	2% (2)
Ring ozone filling–in	+2%
I_o effect	-0.2%

(1) from Kerridge *et al.* (2002); de Beek *et al.* (2003)
(2) from GDP V3 VALREPORT (2002)

9 Summary and Conclusion

A novel type of DOAS ozone retrieval algorithm has been successfully implemented for the retrieval of total ozone from GOME. This new algorithm has been termed weighting function DOAS (WF-DOAS) and it permits the direct fitting of vertical column densities. It is particularly suited for the retrieval in spectral regions with strong absorbers (Buchwitz *et al.*, 2000). In order to reduce the computational burden all radiative transfer model quantities have been prepared in form of look-up-tables. The processing speed is about 5 minutes for a GOME orbit ($\sim$2000 ground pixels) on a SUN Ultra II. From an extensive error analysis it was concluded that WF-DOAS can retrieve GOME total ozone with a precision of 3% for solar zenith angles below 80°.

An important element of the new retrieval scheme was the attempt to incorporate other important geophysical parameters from GOME such as cloud parameters (cloud fraction and cloud-top-height from the oxygen A–band) and, for the first time, the effective albedo from a spectral region containing negligible amount of absorbers near 377 nm. From the cloud information derived from FRESCO (Koelemeijer *et al.*, 2001) an effective scene height is estimated that represents an effective lower boundary of the atmosphere approximating the mixed cloud scene.

Another important aspect that has been accounted for in the retrieval is the ozone filling-in due to the Ring effect. Neglecting this effect can lead to systematic errors on the order of a few percent. In the WF-DOAS V1.0, a-priori information on ozone profile shape is taken from the TOMS V7 climatology (Wellemeyer *et al.*, 1997) that is currently used in the retrieval of total ozone from TOMS. Since this climatology was built from data in the late eighties, a more updated climatolgy is planned to replace the current one.

As an example to see how well WF-DOAS is working in its Version 1.0, comparisons have been made with collocated groundbased measurements done with Dobson and a single monchromator Brewer spectrometer at Hradec Kralove, Czech Republic, 50.2°N, 15.8°E (Vanicek, 1998). Collocation criteria for GOME overpasses was 160 km between the centre coordinate of the GOME pixel and station location and, secondly simultanous measurements of Brewer and Dobson at the same day are available. For a given day only the closest GOME overpass has been selected. For the period 1996-1999 about 300 measurement triples were found fulfilling this criterion. The difference between GOME and the Brewer is shown in Figure 9.1 as a function of the day in the year (from January to December).

No bias (0.1%) between both data sets (WF-DOAS V1.0 and Brewer) is observed and the RMS scatter of differences is 2.5% (second panel). Also shown are the differences of the GDP V3.0 results that are on average 1.3% lower than the Brewer results (third panel in Fig. 9.1). A seasonal cycle in the GDP V3 - Brewer differences is recognisable. One has to keep in mind that the simultanous measurements fom the daily mean Brewer and Dobson data also show a distinct seasonal cycle of up to $\pm$2%. In the accompanying validation report these differences between both GOME analyses and between simultaneous Dobson and Brewer measurements will be discussed in more detail.

The comparison with the Brewer and Dobson data show a significant improvement in the scattering of the GOME differences (from 3.2% in GDP V3.0 to 2.4% in WF-DOAS). A small seasonal signature is observed in the WF-DOAS differences when compared wih the Dobson measurements and this is most likely due to the

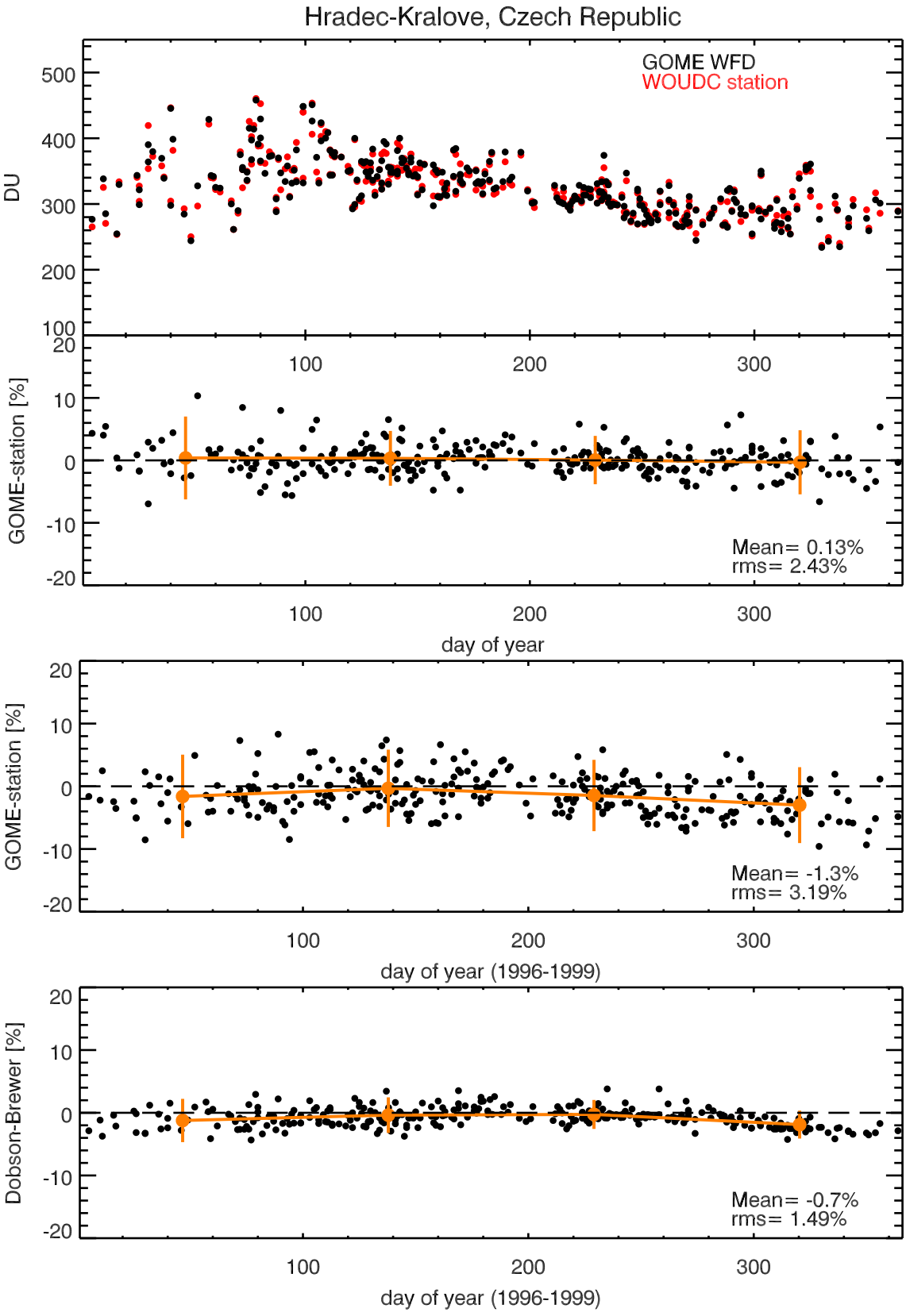

Figure 9.1: *Top: GOME WF-DOAS V1.0 total ozone (black) and collocated Brewer measurements from Hradec-Kralove, Czech Republic (red) from 1996–1999. Second panel: differences between WF-DOAS V1.0 and Brewer in percent. Third panel: differences between GDP V3.0 and Brewer. Bottom panel: Difference between Dobson and Brewer data measured the same day and collocated with GOME overpasses. Orange points with error bars indicate means for each three month period and corresponding 2σ RMS.*

use of a fixed temperature for the ozone cross-section in the standard retrieval of Dobson data, that to a lesser extent also affects the Brewer retrieval.

The major improvement in the WF-DOAS RMS scatter is most likely the result of various new features introduced in the retrieval: ozone Ring filling-in and the use of GOME derived effective albedo and effective scene height.

Acknowledgment

We thank Michel van Roozendael (BIRA) for stimulating discussions on GOME DOAS issues. He also kindly provided us the I_o corrected ozone cross-sections. We are also grateful to Werner Thomas and Diego Loyola, DLR Oberpfaffenhofen, for informations related to GDP V3.0 total ozone retrieval. Karel Vanicek, Czech Hydrological Institute, provided us Dobson and Brewer data from Hradec-Kralove that has been used to compare our results. He also gave us valuable information on the operation of the groundbased instruments. We acknowledge the help of our colleague Andreas Richter, with whom we had many discussions relating to this work.

Appendix

A TOMS V7 ozone profile climatology

The following three figures show the TOMS V7 ozone profile climatology (Wellemeyer *et al.*, 1997) as number density profiles as used in WF-DOAS. Figures A.1, A.2, and A.3 show the profiles for the three latitude bands tropics (0°–30°), mid-latitudes (30°–60°), and high latitudes (60°–90°), respectively.

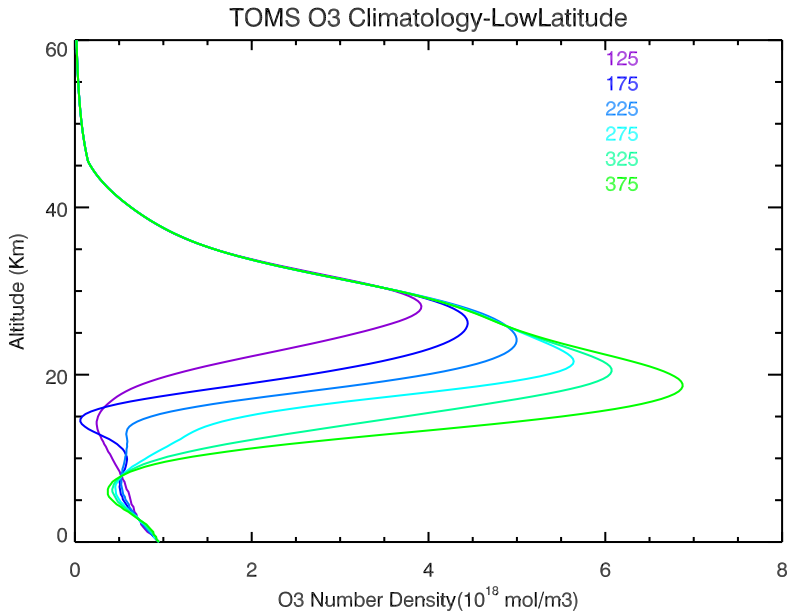

Figure A.1: *TOMS V7 climatological profiles as a function of total ozone. Low latitude zone (LOW_LAT).*

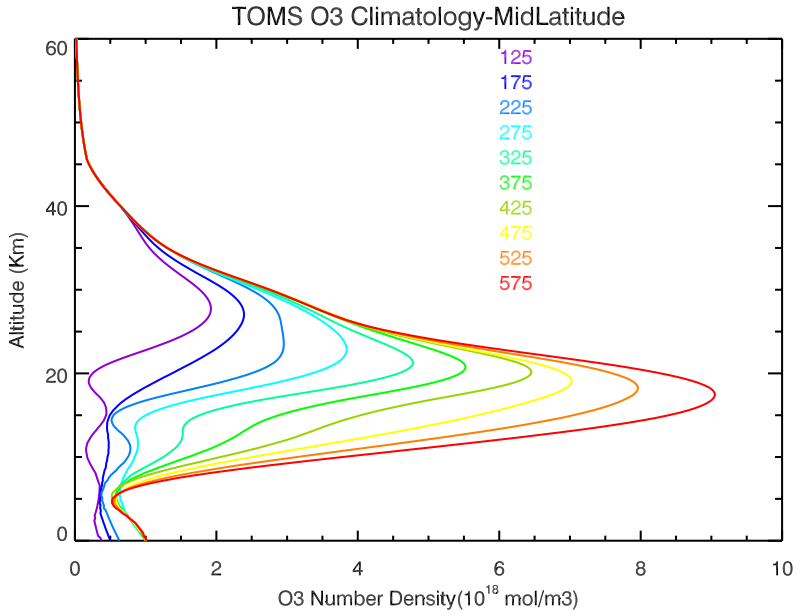

Figure A.2: *TOMS V7 climatological profiles as a function of total ozone. Mid latitudes (MID_LAT).*

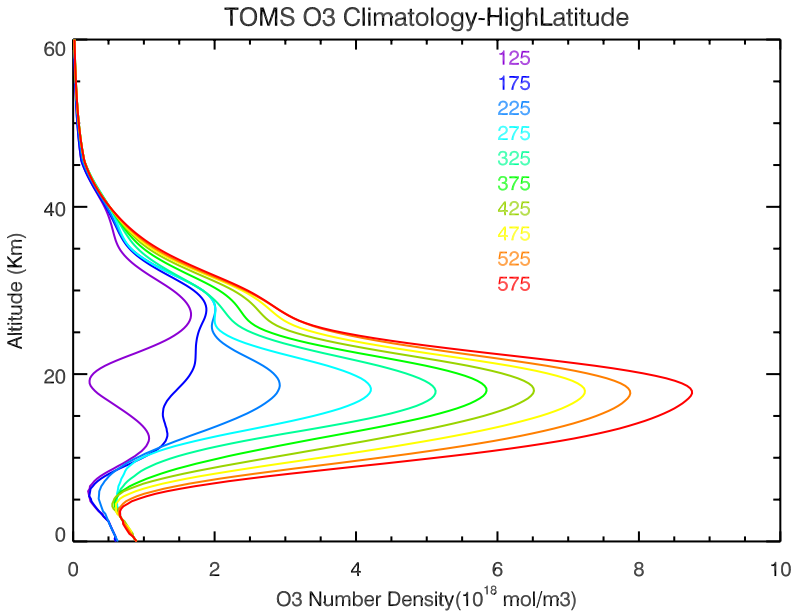

Figure A.3: *TOMS V7 climatological profiles as a function of total ozone. High Latitudes (HIGH_LAT).*

B Acronyms

ACRONYM	MEANING
AMF	AIRMASS FACTOR
ATBD	ALGORITHM THEORETICAL BASIS DOCUMENT
CDI	COMBINED DIFFERENTIAL INTEGRAL
DFD	GERMAN REMOTE SENSING DATA CENTRE
DLR	GERMAN AEROSPACE CENTER
DOAS	DIFFERENTIAL OPTICAL ABSORPTION SPECTROSCOPY
DOD	DIFFERENTIAL OPTICAL DEPTH
EP-TOMS	EARTH PROBE - TOTAL OZONE MAPPING EXPERIMENT
ERS-2	SECOND EUROPEAN REMOTE SENSING SATELLITE
ESA	EUROPEAN SPACE AGENCY
EUMETSAT	EUROPEAN ORGANISATION FOR THE EXPLOITATION OF METEOROLOGICAL SATELLITES
FRESCO	FAST RETRIEVAL SCHEME FOR CLOUDS FROM THE OXYGEN A-BAND
FURM	FULL RETRIEVAL METHOD
GDP	GOME DATA PROCESSOR
GOME	GLOBAL OZONE MONITORING EXPERIMENT
GOTOCORD	GOME TOTAL COLUMN RETRIEVAL DEVELOPMENT
GSAC	GOME SCIENCE ADVISORY COMMITTEE
GVC	GHOST VERTICAL COLUMN
ICFA	INITIAL CLOUD FITTING ALGORITHM
ISCCP	INTERNATIONAL SATELLITE CLOUD CLIMATOLOGY PROJECT
ITCZ	INNER TROPICAL CONVERGENCE ZONE
IUP	INSTITUTE OF ENVIRONMENTAL PHYSICS
LER	LAMBERTIAN EQUIVALENT REFLECTIVITY
LOS	LINE-OF-SIGHT
LUT	LOOK-UP-TABLE
OMI	OZONE MONITORING INSTRUMENT
RRS	ROTATIONAL RAMAN SCATTERING
RTM	RADIATIVE TRANSFER MODEL
SCD	SLANT COLUMN DENSITY
SCIAMACHY	SCANNING IMAGING ABSORPTION SPECTROMETER FOR ATMOSPHERIC CHARTOGRAPHY
SOST	SCIAMACHY OPERATIONS SUPPORT TEAM
SRD	SOFTWARE REQUIREMENTS DOCUMENT
SZA	SOLAR ZENITH ANGLE
TOA	TOP OF ATMOSPHERE
TOMS	TOTAL OZONE MAPPING SPECTROMETER
UV	ULTRAVIOLET
UTC	UNIVERSAL TIME CONSTANT (GREENWICH MERIDIAN TIME)
VCD	VERTICAL COLUMN DENSITY
WF-DOAS	WEIGHTING FUNCTION DOAS
WMO	WORLD METEOROLOGICAL ORGANIZATION
WOUDC	WORLD OZONE AND ULTRAVIOLET RADIATION DATA CENTRE

References

ALIWELL, S. R., ROOZENDAEL, M. VAN, JOHNSTON, P. V., RICHTER, A., WAGNER, T., ARLANDER, D. W., BURROWS, J. P., FISH, D. J., JONES, R. L., TORNKVIST, K. K., LAMBERT, J.-C., PFEILSTICKER, K., and PUNDT, I. 2002. Analysis for BrO in zenith-sky spectra: An intercomparison exercise for analysis improvement. *J. Geophys. Res.* doi:10.1029/2001JD000329.

BOVENSMANN, H., BURROWS, J. P., BUCHWITZ, M., FRERICK, J., NOEL, S., ROZANOV, V.V., CHANCE, K. V., and GOEDE, A. H. P. 1999. SCIAMACHY - Mission objectives and measurement modes. *J. Atmos. Sci.*, **56**, 125–150.

BRAMSTEDT, K., GLEASON, J., LOYOLA, D., THOMAS, W., BRACHER, A., WEBER, M., and BURROWS, J. P. 2003. Comparison of total ozone from the satellite instruments gome and toms with measurements from the dobson network 1996–2000. *Atmos. Chem. Phys.*, **3**, 1409–1419.

BUCHWITZ, M., ROZANOV, V.V., and BURROWS, J.P. 2000. A near-infrared optimized DOAS method for the fast global retrieval of atmospheric CH_4, CO, CO_2, H_2O, and N_2O total column amounts from SCIAMACHY Envisat-1 nadir radiances. *J. Geophys. Res.*, **105**, 15,231–15,245.

BURROWS, J. P., DEHN, A., DETERS, B., HIMMELMANN, S., RICHTER, A., VOIGT, S., and ORPHAL, J. 1998. Atmospheric remote-sensing reference data from GOME: Part 1. Temperature-dependent absorption cross sections of NO_2 in the 231-794 nm range. *J. Quant. Spectrosc. Rad. Transfer*, **60**, 1025–1031.

BURROWS, J. P., RICHTER, A., DEHN, A., DETERS, B., HIMMELMANN, S., VOIGT, S., and ORPHAL, J. 1999a. Atmospheric remote-sensing reference data from GOME: Part 2. Temperature-dependent absorption cross sections of O_3 in the 231-794 nm range. *J. Quant. Spectrosc. Rad. Transfer*, **61**, 509–517.

BURROWS, J.P., CHANCE, K.V., GOEDE, A.P.H., GUZZI, R., KERRIDGE, B.J., MULLER, C., PERNER, D., PLATT, U., POMMEREAU, J.-P., SCHNEIDER, W., SPURR, R.J.D., and VAN DER WOERD, H. 1993. *Global Ozone Monitoring Experiment: Interim Science Report*. Tech. rept. ESA, ESTEC, Publication Divisions, Noordwijk, The Netherlands. ESA Special Publication 1151.

BURROWS, J.P., WEBER, M., BUCHWITZ, M., ROZANOV, V.V., LADSTÄDTER-WEISSENMAYER, A., RICHTER, A., DE BEEK, R., HOOGEN, R., BRAMSTEDT, K., EICHMANN, K.-U., EISINGER, M., and PERNER, D. 1999b. The Global Ozone Monitoring Experiment (GOME): Mission concept and first scientific results. *J. Atmos. Sci.*, **56**, 151–175.

CHANCE, K., and SPURR, R. J. D. 1997. Ring effect studies: Rayleigh scattering, including molecular parameters for rotational Raman scattering and the Fraunhofer spectrum. *Appl. Opt.*, **36**, 5224 – 5230.

COLDEWEY-EGBERS, M., WEBER, M., BUCHWITZ, M., and BURROWS, J.P. 2003. Application of a modified DOAS method for ozone retreival from GOME data at high polar latitude. *Adv. Space Res.* in press.

DE BEEK, R., VOUNTAS, M., ROZANOV, V. V., RICHTER, A., and BURROWS, J. P. 2001. The Ring effect in the cloudy atmosphere. *Geophys. Res. Lett.*, **28**, 721–724.

DE BEEK, R., WEBER, M., ROZANOV, V.V., ROZANOV, A., RICHTER, A., and BURROWS, J.P. 2003. Trace gas column retrieval – an error study for GOME-2. *Adv. Space Res.* in press.

FISH, D.J., and JONES, R.L. 1995. Rotational Raman scattering and the Ring effect in zenith-sky spectra. *Geophys. Res. Lett.*, **22**, 712–716.

GDP V3 VALREPORT. 2002. *ERS-2 GOME GDP 3.0 implementation and delta validation report*. Technical Note ERSE-DTEX-EOAD-TN-02-0006, Issue 1.0, November 2002, ed. J.–C. Lambert, see also: http://earth.esrin.esa.it/pub/ESA_DOC/GOME/gdp3/gdp3.htm.

GOME LVL2. 2000. GOME level 1 to 2 algorithms descriptions. *Tech. Rep. ER-TN-DLR-GO-0025, Issue 2B*. prepared by R. Spurr and W. Thomas, http://atmos.af.op.dlr.de/cgi-bin/home.cgi?page=projdocs.

GRAINGER, J.F., and RING, J. 1962. Anomalous Fraunhofer line profiles. *Nature*, **193**, 762–762.

HARE, E., and FIOLETOV, V. 1998. An examination of the total ozone data in the World Ozone and Ultraviolet Radiation Data Center. *Pages 45–48 of:* BOJKOV, R., and VISCONTI, G. (eds), *Atmospheric ozone - proc. 18th quadrennial ozone symposium, l'aquila, italy*.

HERMAN, J.R., and CELARIER, E.A. 1997. Earth surface reflectivity climatology at 340-380 nm from TOMS data. *J. Geophys. Res.*, **102**(D23), 28003–28011.

HOOGEN, R., ROZANOV, V. V., and BURROWS, J. P. 1999. Ozone profiles from GOME satellite data: Algorithm description and first validation. *J. Geophys. Res.*, **104**, 8263–8280.

HSU, N.C., HERMAN, J. R., TORRES, O., HOLBEN, B. N., TANRE, D., ECK, T. F., SMIRNOV, A., CHATENET, B., and LAVENU, F. 1999. Comparisons of the TOMS arorosol index with sun-photometer aerosol optical thickness: Results and applications. *J. Geophys. Res.*, **104**, 6269–6280. 10.1029/1998JD200086.

JOINER, J., and BHARTIA, P. K. 1995. The determination of cloud pressures from rotational Raman scattering in satellite backscatter ultraviolet measurements. *J. Geophys. Res.*, **100**, 23019–23026.

JOINER, J., BARTHIA, P.K., CEBULA, R.P., HILSENRATH, E., MCPETERS, R.D., and PARK, H. 1995. Rotational Raman scattering (Ring effect) in satellite backscatter ultraviolet measurements. *Applied optics*, **34**, 4513–4525.

KATTAWAR, G.W., YOUNG, A.T., and HUMPHREYS, T.J. 1981. Inelastic scattering in planetary atmospheres, I, the Ring effect, without aerosols. *Astrophys. J.*, **243**, 1049–1057.

KERRIDGE, B., SIDDANS, R., LATTER, B., BURROWS, J.P., WEBER, M., DE BEEK, R., RICHTER, A., ROZANOV, V.V., ABEN, I., TANZI, C., HARTMANN, W., and WICKETT, M.G. 2002. *GOME-2 Error assessment study*. Tech. rept. Eumetsat Contract: EUM/CO/01/901/DK.

KOELEMEIJER, R.B.A., STAMMES, P., HOVENIER, J.W., and DE HAAN, J.F. 2001. A fast method for retrieval of cloud parameters using oxygen A-band measurements from the Global Ozone Monitoring Experiment. *J. Geophys. Res.*, **106**, 3475–3496.

KOELEMEIJER, R.B.A., DE HAAN, J. F., and STAMMES, P. 2003. A database of spectral surface reflectivity in the range 335–772 nm derived from 5.5 years of GOME observations. *J. Geophys. Res.*, **108**. doi:10.1029/2002JD002429.

KURUCZ, R.L., FURENLID, I., BRAULT, J., and TESTERMAN, L. 1984. *Solar flux atlas from 296 nm to 1300 nm*. National Solar Obswervatory, Sunspot, New Mexico.

LAMBERT, J.C., VAN ROOZENDAEL, M., DE MAZIERE, M., SIMON, P.C., POMMERAU, J.-P., GOUTAIL, F., SARKISSIAN, A., and GLEASON, J.F. 1999. Investigation of pole-to-pole performances of space-borne atmospheric sensors with ground-based networks. *J. Atmos. Sci.*, **56**, 176–XXX.

LAMBERT, J.C. *,et al.* 1995. Combined characterisation of GOME and TOMS total ozone measurements from space using ground-based observations from NDSC. *Adv. Space Res.*, **35**, 445–451.

MENKHAUS, A., WEBER, M., HAITE, C., and BURROWS, J.P. 1999. Surface UV modelling using GOME data. *Pages 325–332 of: European symposium on atmospheric measurements from space, proc. esams'99*. ESA-WPP-161. European Space Agency.

PLATT, U., and PERNER, D. 1980. Direct measurements of atmospheric hcho, hono, o_3, no_2, and so_2 by differential optical absorption in the near UV. *J. Geophys. Res.*, **85**, 7453–XXXX.

RICHTER, A., and WAGNER, T. 2001. *Diffuser plate spectral structures and their influence on GOME slant columns*. Technical Note, see http://www.iup/gome/data/diffuser_gome.pdf.

RICHTER, A., WITTROCK, F., EISINGER, M., and BURROWS, J.P. 1998. GOME observations of tropospheric BrO in northern hemispheric spring and summer 1997. *Geophys. Res. Lett.*, **25**, 2683–2686.

ROOZENDAEL, M. VAN, SOEBIJANTA, V., FAYT, C., and LAMBERT, J.-C. 2003. *Investigation of DOAS issues affecting the accuracy of the GDP version 3.0 total ozone product*. unpublished manuscript, see Chapter VI of http://earth.esrin.esa.it/pub/ESA_DOC/GOME/gdp3/gdp3.htm.

ROZANOV, V.V., D.DIEBEL, SPURR, R.J.D., and BURROWS, J.P. 1997. GOMETRAN: A radiative transfer model for the satellite project GOME, The plane-parallel version. *J. Geophys. Res.*, **102**(D14), 16683–16695.

ROZANOV, V.V., KUROSU, T., and BURROWS, J.P. 1998. Retrieval of atmospheric constituents in the UV/visible: A new analytical approach to calculating weighting functions. *J. Quant. Spectrosc. Rad. Transfer*, **60**, 277–299.

SHETTLE, E.P., and FENN, R.W. 1976. Models of the atmospheric aerosolsand their optical properties. *In: Agard conference proceedings no.183, ada 028-615*.

SHETTLE, E.P., and FENN, R.W. 1979. Models of the aerosols of the lower atmosphere and the effects of humidity variations on their optical properties. *In: Afgl-tr-79-0214, ada 085951*.

SLIJKHUIS, S., V. BARGEN, A., THOMAS, W., and K.V.CHANCE. 1999. Calculation of Undersampling correction spectra for DOAS spectral fitting. *Pages 563–569 of:* ESA (ed), *Esams'99 - european symposium on atmospheric measurements from space*. ESA, Noordwijk, The Netherlands.

SOLOMON, S., SCHMELTEKOPF, A.L., and SANDERS, R.W. 1987. On the interpretation of zenith-sky absorption measurements. *J. Geophys. Res.*, **92**, 8311–8319.

STAMMES, P., LEVELT, P., DE VRIES, J., VISSER, H., KRUIZINGA, B., SMORENBURG, C., LEPPELMEIER, G., and HILSENRATH, E. 1999. Scientific requirements and optical design of the Ozone Monitoring Instrument on EOS-CHEM. *Pages 221–232 of: Proceedings of SPIE Conference on Earth Observing Systems IV, July 1999, Denver, Colorado, USA*, vol. SPIE 3750.

VANICEK, K. 1998. Differences between Dobson and Brewer observations of total ozone at Hradec-Kralove. *Pages 81–84 of:* BOJKOV, R.D., and VISCONTI, G. (eds), *Atmospheric Ozone, Proc. Quadr. Ozone Symp.* Edigrafital S.p.A.-S.Atto (TE).

VOUNTAS, M., ROZANOV, V.V., and BURROWS, J.P. 1998. Ring effect: Impact of rotational raman scattering on radiative transfer in earth's atmosphere. *J. Quant. Spectrosc. Radiat. Transfer*, **60**, 943–961.

WELLEMEYER, C. G., TAYLOR, S. L., SEFTOR, C. J., MCPETERS, R. D., and BHARTIA, P. K. 1997. A correction for the Total Ozone Mapping Spectrometer profile shape errors at high latitude. *J. Geophys. Res.*, **102**, 9029–9038.

WMO REPORT. 1999. *Scientific Assessment of Ozone Depletion: 1998*. World Meteorological Organization, Gobal Ozone Research and Monitoring Project, Report No. 44.